Accurate modeling of the dynamics of dissociative chemisorption on metal surfaces

Gerrits, N.

Chapter 4

Large Effect of Rotational Pre-excitation of HCl on its Reaction on Au(111): A Rotational Phase Lock-in Effect

This chapter is based on Gerrits, N.; Geweke, J.; Auerbach, D. J.; Beck, R. D.; Kroes, G.-J. Highly Efficient Activation of HCl Dissociation on Au(111) via Rotational Preexcitation. *J. Phys. Chem. Lett.* **2021**, *12*, 7252–7260, DOI: 10.1021/acs.jpclett.1c02093

Abstract

Dissociative chemisorption of molecules on metal surfaces, which is relevant to heterogeneous catalysis, can be subject to important non-statistical effects. Cases have been recorded in which adding energy to the molecule's vibration promotes reaction more effectively than increasing the collision energy, but similar results have not yet been presented for rotational pre-excitation. In this chapter, it is shown that adding energy to the rotation of HCl can promote its dissociation on Au(111) 20 times more effectively than increasing its translational energy. Our prediction can be tested by experiments within the present state-of-the-art. In the underlying mechanism the molecule needs to rotate initially in the polar angle θ of its orientation relative to the surface so that it can pass through a critical region of the reaction path in a region in front of the barrier, where this path shows a strong and non-monotonic dependence on θ.

4.1 Introduction

Fundamental understanding of molecule-metal surface reaction (MMSR) mechanisms is vital for heterogeneous catalysis as MMSRs play an important role in many industrial processes[1–5]. The efficiency or the rate of an industrial heterogeneously catalyzed process, which consists of a sequence of elementary surface reactions, is often controlled[6] by the transition state (TS) of a dissociative chemisorption reaction on a metal surface[6–8], as is the case in ammonia production[2] and steam reforming[3]. However, not only statistical effects, which can be associated with the TS, but also dynamical effects on the dissociation reaction can play an important role in an MMSR[9–28].

An important example of dynamical effects on dissociative chemisorption reactions is mode-specifity. For instance, many[29–31], although not all dissociative chemisorption reactions[32], display sticking probabilities that depend only on the fraction of the molecule's translational energy that is normal to the surface (normal energy scaling, NES). Putting additional vibrational energy in an incident molecule usually increases its reaction probability, with an efficacy that differs from that achieved by enhancing its incident translational energy by the same amount[9–14, 17, 18, 33–35]. For some systems, increasing the vibrational energy is even more effective at increasing the reaction probability than increasing the translational energy, in which case we say that the vibrational efficacy exceeds one[10, 17, 21, 22, 25, 34, 35] (see also Chapters 3 and 8 to 10). In contrast, increasing the rotational energy of a molecule incident on a metal surface is usually not very effective at increasing the reaction probability, and to the best of our knowledge the rotational efficacy has always been found to be lower than one: adding rotational energy is less effective at promoting reaction than adding the same amount of translational energy. For example, in the benchmark MMSR of H_2 + Cu(111) rotational energy only has a small influence on the dissociation probability[30, 31, 36, 37] (the rotational efficacy is 0.3 - 0.5[30, 31]), and a similar effect has been observed for H_2 on other metal surfaces[38–42]. In the mechanism found to be operative for H_2 reacting on coinage metal surfaces, rotational energy is converted to energy in motion along the reaction path because the rotational constant of the molecule decreases as its bond length extends upon approaching the late barrier[30, 31]. Adding rotational energy has an even smaller effect on the sticking of methane on Ni(111)[43]. Moreover, rotational effects are not expected to be easily visible in molecular beam experiments on sticking of small molecules not containing hydrogen atoms: these molecules tend to have small rotational constants, so that rotational cooling should be very efficient in such molecular beams[44–47].

The dissociative chemisorption of HCl on Au(111) has been called an enigmatic reaction[48] for several reasons. For example, the first measured sticking probabilities[49] were found to exceed previously predicted values[50] by about two orders of magnitude, and the analysis of the experiments suggested a very high vibrational efficacy. Subsequent dynamics calculations managed to reduce the discrepancies between computed and measured S_0 values, but the computed S_0 still exceeded the measured values by one order of magnitude[48, 51, 52]. Only recently considerably better agreement between theory and experiment was achieved for sticking at normal incidence[25] (see Chapter 3). The improved agreement resulted from the theory using a better density functional (the MS-RPBEl meta-GGA functional[53]), and a reanalysis of the experiments concerning, for instance, the relationship between the sticking probability and the Auger signals used to establish the coverage of Au by Cl[25]. As a result, the discrepancy between the computed and measured sticking probabilities at normal incidence was reduced to a factor ranging from 2 to 7, depending on the incidence energy. Also, the trends observed experimentally in the energy transfer[54] and (in)elastic scattering probabilities[55] were reproduced qualitatively, suggesting that the new PES should be adequate for describing the reaction mechanism of HCl + Au(111). However, sticking at off-normal incidence and the unusually large vibrational efficacy implicit in a former analysis of the experiments[49] were not yet addressed in Chapter 3.

In this chapter, we consider the sticking of HCl on Au(111) at off-normal incidence, paying special attention to the effects of the rotational temperature of the incident molecular beam and its average incidence energy parallel to the surface. For this, the previous experiments on sticking at off-normal incidence were re-analyzed in the same way as done before for normal incidence[25]. Also, the same improved potential energy surface was used as in the previous successful study on scattering at normal incidence[25] in Chapter 3. For technical details of this chapter, the reader is referred to Chapter 3. The theory based on the meta-GGA functional yields an even better description of sticking at off-normal incidence than obtained for normal incidence[25] in Chapter 3. Surprisingly, the calculations show very high rotational efficacies for reaction, i.e., values exceeding a factor 10. This high rotational efficacy is caused by a strong and non-monotonic dependence of the reaction path on the polar angle θ of the orientation of HCl relative to the Au(111) surface in a region of this path that just precedes the barrier. To traverse this region, the molecule needs to rotate initially, and it needs to arrive at this region with the right rotational phase.

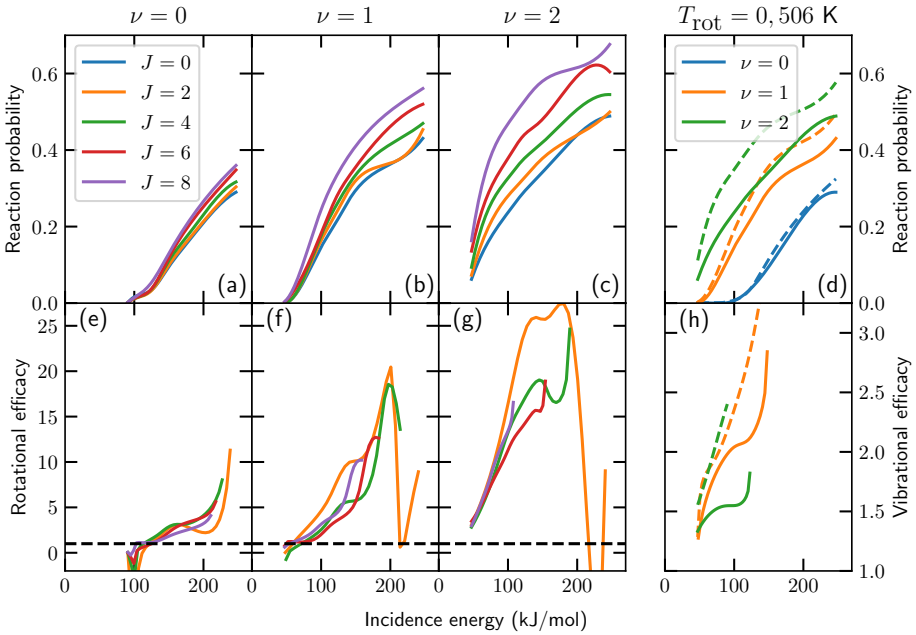

FIGURE 4.1: (a-c) Reaction probability for normally incident HCl on Au(111) and (e-g) the corresponding rotational efficacy. Results for $\nu = 0$ are shown in panels a and d, for $\nu = 1$ in panels b and e, and for $\nu = 2$ in panels c and f. The rotational efficacy is computed relative to $J = 0$ with the same vibrational state. The dashed line indicates a rotational efficacy of unity. (d) Reaction probability and (h) concomitant vibrational efficacy. The vibrational efficacy is computed relative to $\nu = 0$ with the same rotational state distribution. The solid (dashed) lines indicate results for $T_{\mathrm{rot}} = 0\,\mathrm{K}$ ($T_{\mathrm{rot}} = 506\,\mathrm{K}$).

4.2 Results

4.2.1 Rotational and Vibrational Efficacies

For now, we consider normally incident HCl only, dropping the incidence angle from our notation and writing the initial state selected reaction probability simply as $R_{\nu,J}(E_{\mathrm{i}})$, where ν is the initial vibrational and J the rotational quantum number (see also Section 4.C). Figures 4.1a-c show a large dependence of $R_{\nu,J}(E_{\mathrm{i}})$ on J for $\nu = 0, 1$, and especially 2. We may define the rotational efficacy, which measures how effective adding rotational energy is at promoting the reaction (i.e., at achieving an initial state-selected reaction probability

TABLE 4.1: Rotational (χ_J) and vibrational (χ_ν) efficacies of HCl on Au(111) as a function of the reaction probability (Eq. 4.1).

R \ ν	$\chi_{J=2}$			$\chi_{J=4}$			$\chi_{J=6}$			$\chi_{J=8}$			$\chi_\nu(J=0)$		$\chi_\nu(T_{\rm rot}=506\,{\rm K})$	
	0	1	2	0	1	2	0	1	2	0	1	2	$0\to1$	$0\to2$	$0\to1$	$0\to2$
0.05	0.5	2.0	-	1.0	0.8	-	0.6	1.2	-	1.1	1.2	-	1.7	-	1.8	-
0.10	2.2	3.8	5.3	2.2	1.8	3.1	1.4	1.2	-	1.2	1.6	-	1.9	1.4	2.0	-
0.15	3.1	6.5	10.9	3.1	3.1	6.0	2.6	1.6	4.0	1.9	2.2	-	2.0	1.5	2.2	1.7
0.20	2.3	9.8	18.7	3.4	5.0	9.9	3.4	2.8	6.0	2.4	3.1	4.1	2.1	1.5	2.4	1.9
0.25	2.9	10.4	25.3	4.7	5.7	13.9	4.0	3.7	8.4	3.0	3.8	5.9	2.2	1.6	2.7	2.1
0.30	-	14.6	25.7	-	6.6	16.6	-	4.6	10.8	-	4.5	7.9		-	3.1	2.3
0.35	-	19.1	27.5	-	12.3	18.8	-	7.7	13.0	-	6.8	10.1		-		-
0.40	-	3.9	20.2	-	18.3	17.7	-	12.5	14.6	-	9.9	11.9		-		-

equal to R), relative to increasing $E_{\rm i}$ and for HCl in the state ν, as follows:

$$\chi_J(R;\nu) = \frac{E_{\rm i}(\nu, J=0; R) - E_{\rm i}(\nu, J; R)}{E_{\rm rot}(\nu, J) - E_{\rm rot}(\nu, J=0)}. \tag{4.1}$$

Here, $E_{\rm i}(\nu, J; R)$ is the incidence energy at which $R_{\nu,J}(E_{\rm i}) = R$. Table 4.1 shows that rotational efficacies defined in this way may be large, e.g., for $J = 6$ it takes on the values of 4.0 for $\nu = 0$ and $R = 0.25$, of 12.5 for $\nu = 1$ and $R = 0.40$, and of 14.6 for $\nu = 2$ and $R = 0.40$. In writing and applying Eq. 4.1 we have tentatively assumed that $R_{\nu,J}(E_{\rm i})$ is a bijective or invertible function, i.e., only one value of $E_{\rm i}$ corresponds to a particular value of $R_{\nu,J}$. This will usually be true as $R_{\nu,J}(E_{\rm i})$ tends to be a monotonically increasing function of $E_{\rm i}$. We may then also define a function $E_{\rm i}^{\nu,J}(R)$, which is equal to the incidence energy $E_{\rm i}$ at which $R_{\nu,J}(E_{\rm i}) = R$. This allows us to define a rotational efficacy that depends on incidence energy for the molecule in the state ν as follows:

$$\chi_J(E_{\rm i};\nu) = \frac{E_{\rm i}(\nu, J=0; R) - E_{\rm i}(\nu, J; R)}{E_{\rm rot}(\nu, J) - E_{\rm rot}(\nu, J=0)}. \tag{4.2}$$

In Eq. 4.2, the argument $E_{\rm i}$ is the incidence energy for which a reaction probability R is obtained for the higher rotational state. The rotational efficacy defined in this way is plotted in Figures 4.1e-g. The plots show that the rotational efficacy strongly depends on the value of $E_{\rm i}$ at which it is evaluated for the higher rotational state, and it also strongly depends on the value of ν. For example, for $J = 6$ the rotational efficacy takes on values of up to 4 for $\nu = 0$, up to 12 for $\nu = 1$, and up to 20 for $\nu = 2$.

Figure 4.1d also shows a large dependence of $R_{\nu,J}(E_{\rm i})$ on ν for $J = 0$. To determine the effectiveness of vibrational pre-excitation for promoting

reaction, the vibrational efficacies $\chi_\nu(R;J)$ and $\chi_\nu(E_i;J)$ may be defined in a way that is entirely analogous to Eqs. 4.1 and 4.2, respectively. As can be seen from Table 4.1, $\chi_\nu(R;J)$ can also take on large values (for $J=0$, these values are up to 2.2 for $\nu=1$, and up to 1.6 for $\nu=2$), which are considerably larger than one. However, they are much smaller than the values achieved for $\chi_J(R;\nu)$ (e.g., up to 14.6 for $\nu=2, J=6$). This suggests that rotational pre-excitation of the molecules present in a molecular beam may have a greater effect on the sticking probability $S_0(E_i, T_N, \Theta_i)$ measured in a molecular beam experiment than vibrational pre-excitation. We will come back to this different efficacy later. A similar picture emerges from the plots of $\chi_\nu(E_i;J)$, which takes on values of up to 2.8 for $\nu=1$ and up to 1.8 for $\nu=2$, respectively (Figure 4.1h).

Vibrational efficacies may also be evaluated for a thermal rotational distribution instead of for $J=0$ only. In Figure 4.1h, we show $\chi_\nu(E_i;T_{rot}=506\,K)$ for the highest rotational temperature achieved in the recent molecular beam experiments on HCl + Au(111), i.e., $T_{rot}=506\,K$. Here, we see a synergistic effect, i.e., the effects of increased vibrational and rotational pre-excitation are mutually reinforcing, which, to the best of our knowledge, has not been observed before (see also Section 4.F).

In the literature, values of vibrational efficacies have often been based on fits of $R_{\nu,J}(E_i)$ where the fit function is taken as an S-shaped function of E_i, e.g., as a function containing an error function or tanh function of E_i[30, 31, 56–58]. If these functions are taken to be of the same shape (i.e., if they have the same "width" and "saturation value"), the efficacies $\chi_\nu(R;J)$ and $\chi_\nu(E_i;J)$ become independent of R and of E_i, respectively, and the vibrational efficacy may be evaluated simply as

$$\chi_\nu(J) = \frac{E_0(\nu=0,J) - E_0(\nu,J)}{E_{vib}(\nu,J) - E_{vib}(\nu=0,J)}, \tag{4.3}$$

where $E_0(\nu,J)$ is simply defined as the incidence energy at which $R_{\nu,J}(E_i)$ becomes equal to half its maximum value (i.e., its "saturation value"), as achieved at high E_i. One could attempt to extract the vibrational efficacy with the aid of Eq. 4.3 in a procedure where experiments are performed for normal incidence, varying the nozzle temperature to increase the (normal) incidence energy and the vibrational state populations, and for off-normal incidence at a high nozzle temperature, varying the normal incidence energy by varying the incidence angle while keeping the vibrational state populations constant. Such a procedure was recently used to extract $E_0(\nu)$ parameters for $\nu=0$ and 1 for HCl + Au(111), assuming rotational effects to be negligible and assuming

TABLE 4.2: Sticking probabilities for off-normally incident HCl on Au(111) shown in Figure 4.2 for laser-off and laser-on conditions.

E_n (kJ/mol)	$S_0^{\text{laser-off}}$	$S_{0,\nu=1,J=2}^{\text{laser-on}}$	$S_{0,\nu=1,J=8}^{\text{laser-on}}$	$S_{0,\nu=2,J=2}^{\text{laser-on}}$	$S_{0,\nu=2,J=8}^{\text{laser-on}}$
47	0.000 ± 0.000	0.000 ± 0.000	0.000 ± 0.000	0.006 ± 0.000	0.008 ± 0.000
67	0.001 ± 0.000	0.004 ± 0.001	0.004 ± 0.000	0.015 ± 0.001	0.015 ± 0.001
99	0.010 ± 0.001	0.022 ± 0.001	0.021 ± 0.001	0.030 ± 0.001	0.029 ± 0.001
123	0.044 ± 0.002	0.061 ± 0.002	0.060 ± 0.002	0.068 ± 0.002	0.067 ± 0.002
142	0.088 ± 0.003	0.109 ± 0.003	0.106 ± 0.003	0.113 ± 0.003	0.111 ± 0.003
170	0.169 ± 0.004	0.193 ± 0.004	0.191 ± 0.004	0.197 ± 0.004	0.196 ± 0.004
247	0.331 ± 0.005	0.353 ± 0.005	0.351 ± 0.005	0.356 ± 0.005	0.355 ± 0.005

TABLE 4.3: State-specific reaction probabilities for off-normally incident HCl on Au(111) used to compute the laser-off and laser-on sticking probabilities shown in Figure 4.2.

E_n (kJ/mol)	$R_{\nu=0,J=3}$	$R_{\nu=0,J=7}$	$R_{\nu=1,J=2}$	$R_{\nu=1,J=8}$	$R_{\nu=2,J=2}$	$R_{\nu=2,J=8}$
47	0.000 ± 0.000	0.000 ± 0.000	0.001 ± 0.000	0.005 ± 0.001	0.073 ± 0.003	0.163 ± 0.004
67	0.000 ± 0.000	0.000 ± 0.000	0.033 ± 0.002	0.071 ± 0.003	0.183 ± 0.004	0.327 ± 0.005
99	0.006 ± 0.001	0.008 ± 0.001	0.161 ± 0.004	0.243 ± 0.004	0.279 ± 0.005	0.466 ± 0.005
123	0.032 ± 0.002	0.043 ± 0.002	0.236 ± 0.004	0.342 ± 0.005	0.332 ± 0.005	0.531 ± 0.005
142	0.079 ± 0.003	0.095 ± 0.003	0.291 ± 0.005	0.393 ± 0.005	0.369 ± 0.005	0.561 ± 0.005
170	0.158 ± 0.004	0.176 ± 0.004	0.350 ± 0.005	0.460 ± 0.005	0.407 ± 0.005	0.604 ± 0.005
247	0.304 ± 0.005	0.354 ± 0.005	0.453 ± 0.005	0.561 ± 0.005	0.499 ± 0.005	0.676 ± 0.005

S_0 to depend only on normal incidence energy[49]. Applying this procedure blindly using Eq. 4.3 would yield a vibrational efficacy of 6.4 (see Section 4.B and Table 4.B.1), which is considerably higher than the computed efficacy ($\chi_{\nu=1} = 1.8 - 3.1$). We attribute this discrepancy not only to the neglect of rotational effects in the aforementioned procedure to obtain the vibrational efficacy, but also to the procedure used to obtain the effective barrier heights (see Section 4.B).

Our prediction of a high rotational efficacy will of course be most useful if it can be confirmed with experiments within the present state-of-the-art. In Figure 4.2 and Tables 4.2 and 4.3, we show that it is possible to do. To enable excitation to high J, the experiments suggested (see also Section 4.C) would employ a high T_N and off-normal incidence to vary the normal incidence energy, as done before in the off-normal incidence experiments on HCl + Au(111)[49]. Furthermore, the experiments we suggest would pre-excite HCl to the $J = 2$ and $J = 8$ states in $\nu = 1$ or $\nu = 2$, and would therefore be able to verify that the reaction of $J = 8$ HCl is far more efficient than that of $J = 2$ HCl. Specifically, such an experiment would pre-excite HCl to a specific rovibrational state (here, from $\nu = 0$ and $J = 3$ to $\nu = 1$ or 2 and $J = 2$; or from

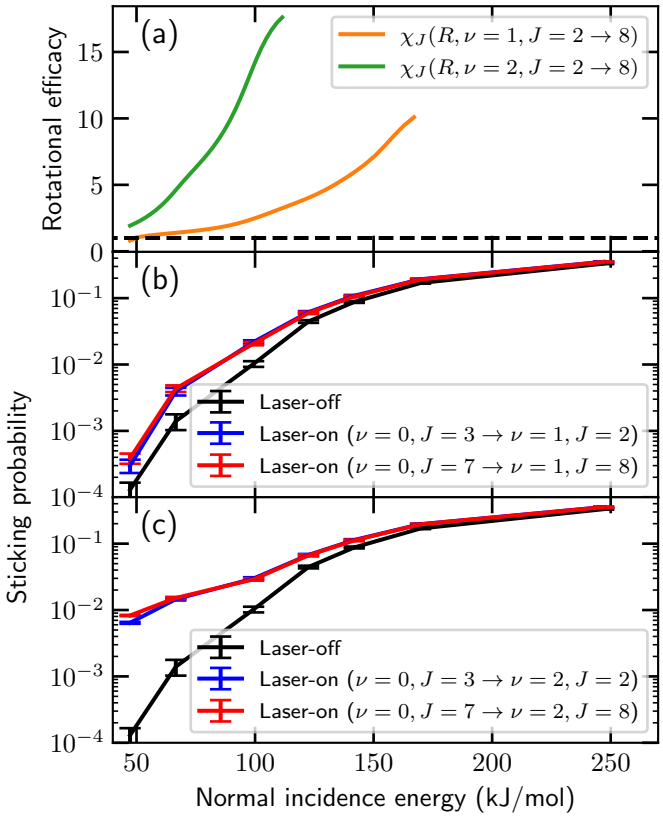

FIGURE 4.2: (a) Predicted rotational efficacy of off-normally incident HCl on Au(111) as a function of normal incidence energy. The $J = 2 \to 8$ rotational efficacy is determined for $\nu = 1$ (orange) and $\nu = 2$ (green). The dashed line indicates a rotational efficacy of unity. (b) Sticking probability of off-normally incident HCl on Au(111) as a function of normal incidence energy. The black lines indicate "laser-off" results for $T_{\text{vib}} = 1060\,\text{K}$ and $T_{\text{rot}} = 506\,\text{K}$. "Laser-on" results, where part of the molecules in the $\nu = 0, J = 3$ ($\nu = 0, J = 7$) state are excited to the $\nu = 1, J = 2$ ($\nu = 1, J = 8$) state, are indicated by the blue (red) lines. The error bars represent 68% confidence intervals. (c) Same as panel b, except that the laser-on results are for the $\nu = 2, J = 2$ and $\nu = 2, J = 8$ excited states.

$\nu = 0$ and $J = 7$ to $\nu = 1, 2$ and $J = 8$) with a laser. Then, from the "laser-off" and "laser-on" results, a state-specific sticking probability can be obtained (for the procedure see Section 4.C). Note that we have also accounted for the excitation efficiency in such an experiment. For incidence energies below the barrier height (i.e., 100 kJ/mol), the differences between the laser-off and laser-on results are likely to be measurable, especially for $\nu = 2$ (Figure 4.2c). For incidence energies above the barrier height, the differences between the laser-on and laser-off results are small and likely difficult to measure. Fortunately, since it is probable that the employed DF underestimates the barrier height compared to experiment (with an estimated 30 - 50 kJ/mol)[25], a considerably larger range of incidence energies where the state-specific sticking probability is measurable should be available for such an experiment than predicted here.

4.2.2 Reaction Mechanism

We now turn to the cause of the high rotational efficacy. Our explanation is based on the following remarkable observations. First of all, results for $\nu = 0$ and $\nu = 2$ at $E_i = 247$ kJ/mol show that $S_{\nu,J}(\theta)$ is non-zero for all initial values of the polar orientation angle of HCl for all J-values except for $J = 0$ (Figures 4.3a and 4.E.3). This already suggests a partial explanation for the high rotational efficacy: Reaction of molecules with high J is comparatively efficient, because reaction of $J = 0$ HCl is notoriously inefficient. Similarly, vibrational efficacies > 1 are only observed if the reaction of a molecule in $\nu = 0$ is remarkably inefficient, as found in cases where the reaction of molecules in the vibrational ground state is hampered by the bobsled effect[10, 22] (see also Chapters 8 and 9).

Another intriguing observation is that $S_{\nu,J=6}(\theta)$ is larger for $\theta < 90°$ than for $\theta > 90°$ (Figures 4.3a and 4.E.3), even though the barrier for reaction is at $\theta \geq 113°$ for reaction at the top, bridge, fcc, and hcp sites, and at the global TS geometry (which occurs close to, but not at the top site, see Chapter 3)[25]. Note that $\theta = 0°$ corresponds to the H atom pointing away from the surface, and $\theta = 180°$ to the H atom pointing to the surface. Furthermore, independent of the vibrational state, whether or not molecules with $J = 6$ stick not only depends on the initial value of θ, but also on its conjugate momentum, i.e., the sense of rotation (see Figures 4.3b and 4.E.4-4.E.6). This is even more obvious for the $J = 2$ states of $\nu = 0$, 1, and 2 (see Figures 4.E.4 to 4.E.6). These observations suggest that reaction is promoted if the molecule is initially rotating and if it approaches the barrier with an appropriate rotational phase. Inspection of how θ varies with the MEP for the TS and the high symmetry top, bridge, and fcc sites (Figure 4.3c) suggests an explanation. On the way

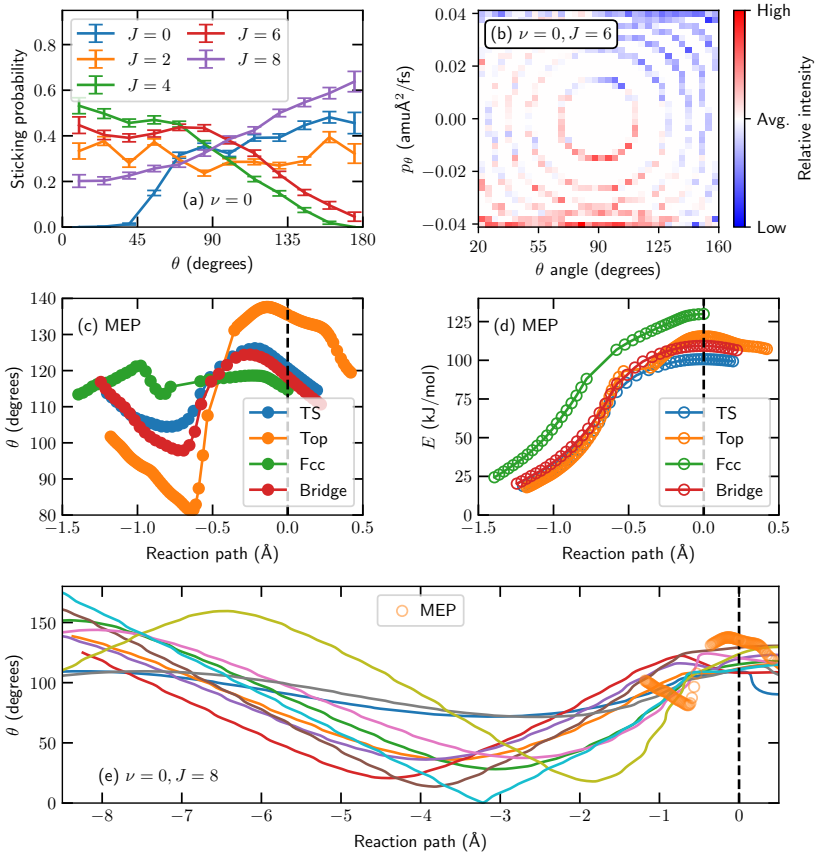

FIGURE 4.3: (a) Sticking probability as a function of the initial θ angle of HCl on Au(111) for $\langle E_i \rangle = 247$ kJ/mol. Results for several rotational states within $\nu = 0$ are shown, which are indicated in the figure. The error bars represent 68% confidence intervals. (b) Distribution of the initial θ angle and its conjugate momentum of reacting HCl on Au(111) for $\nu = 0$ and $J = 6$. The colors indicate the intensity of reactive combinations of θ and p_θ relative to the statistical distribution in the simulated molecular beam; i.e., blue indicates that the combination is less reactive compared to its statistical occurrence whereas red indicates a relatively higher reactivity. The data have been normalized along the θ angle to remove the $\sin\theta$ distribution in the initial statistical distribution, i.e., with the renormalization performed all initial θ angles have equal probability. (c) Polar angle θ of HCl on Au(111) along the MEP of the global TS (blue), and the top (orange), fcc (green), and bridge (red) sites. The black dashed line indicates the TS, i.e., the value of the reaction path is zero. (d) Same as panel c, but showing the potential energy instead of θ. (e) θ angle along the reaction path for a few representative trajectories reacting at the top site for $\nu = 0$ and $J = 8$. The θ angle along the MEP for the top site is indicated by the orange red circles. The black dashed line indicates the location of the reaction barrier, where $r = r^\ddagger = 1.89$ Å[25].

to the barrier, θ depends on the reaction coordinate in a clear non-monotonic manner, especially for the top, TS, and bridge MEPs. The optimal θ value first decreases with the reaction coordinate, then it sharply increases, after which it decreases again, before the molecule reaches the minimum barrier geometry (Figure 4.3c). For the initially non-rotating molecules, "steering" (i.e., the effect that the molecule is steered to the most favorable orientation for reaction by the forces acting on it[59]) cannot take place under these conditions, because the molecule will "overshoot" its most favorable orientation once the most favorable value of θ starts changing in the opposite direction, due to the angular momentum the molecule has acquired. Hence, steering, which can be especially effective for an initially non-rotating molecule[59], will be counterproductive, and on a relative basis molecules with $J = 0$ will be non-reactive. Rather the opposite is observed: the faster the molecule is rotating initially, the higher the probability is that the molecule arrives at the barrier with an appropriate rotational phase (i.e., orientation and angular momentum) to react (see Figures 4.3e and 4.E.7). In chapter 3, it has been found[25] that the top site is relatively unreactive, whereas the hollow site is relatively reactive, even though the barrier heights would suggest the opposite (Figure 4.3d). The strong non-monotonic dependence of the most favorable value of θ on the reaction coordinate is observed to a lesser extent at the fcc site than at the other sites (Figure 4.3c), suggesting that the behaviour of the θ angle along the MEP plays an important role in the dynamical accessibility of the TS, hence also the observed site-specific reactivity in Chapter 3 (i.e., bridge $\geq$ hollow $>$ top).

Our admittedly tentative explanation of the non-monotonic dependence of the value of θ on the reaction path observed for most impact sites is as follows. We suspect that the initial bonding of the dissociating molecule to the surface goes via the more electronegative Cl atom; its increasingly attractive interaction with the surface and the purely repulsive interaction of the H atom with the surface could explain why θ decreases initially with the reaction path coordinate in Figure 4.3c for all sites but the fcc site. For long enough distance between the H and Cl atoms, the H atom will also start bonding with the surface, which can explain the increase in the θ value of the reaction path starting at the value of roughly -0.6 Å of the reaction path coordinate in Figure 4.3c.

4.2.3 Sticking Probabilities

We now come back to the possibility that rotational excitation may have a larger effect on S_0 than vibrational excitation. Figures 4.4a,b show the experimental and theoretical sticking probabilities of normally (red diamonds) and

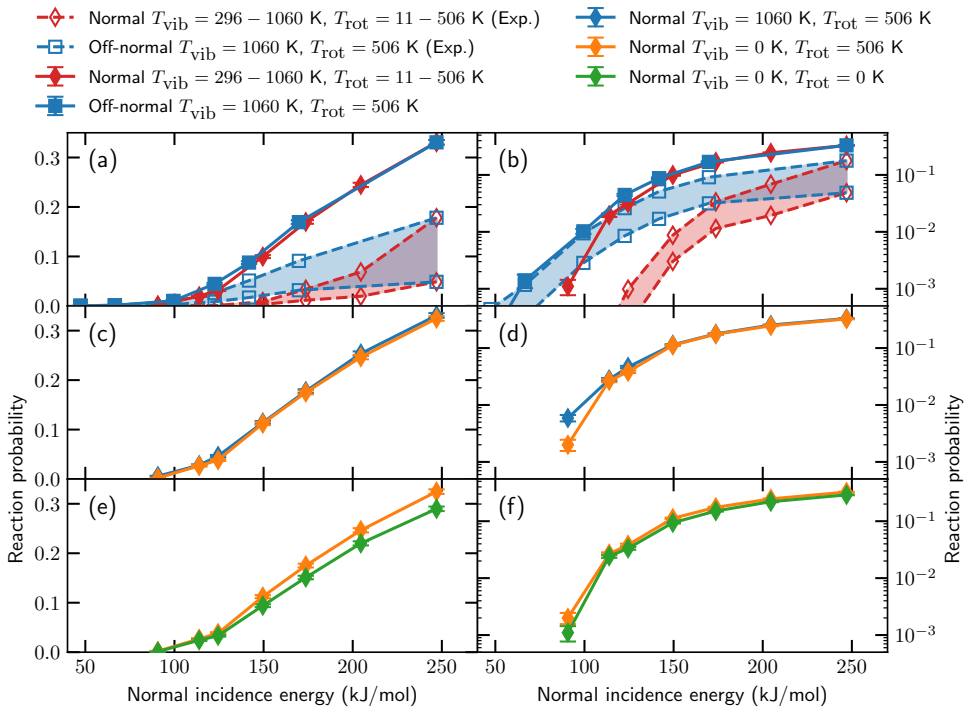

FIGURE 4.4: Sticking probability of HCl on Au(111) as a function of normal incidence energy for various conditions ((off-)normal indicidence, and vibrational and rotational temperatures). The open symbols and dashed lines indicate experimental results, where the shaded area indicates their uncertainty. The solid symbols and lines indicate computed results. The diamonds (squares) are for (off-)normal incidence, where the color indicates the rotational and vibrational temperatures (see legend). The error bars represent 68% confidence intervals. Panels b, d, and f are identical to panels a, c, and e, respectively, except that a logarithmic scale is used instead. For further explanation see the text.

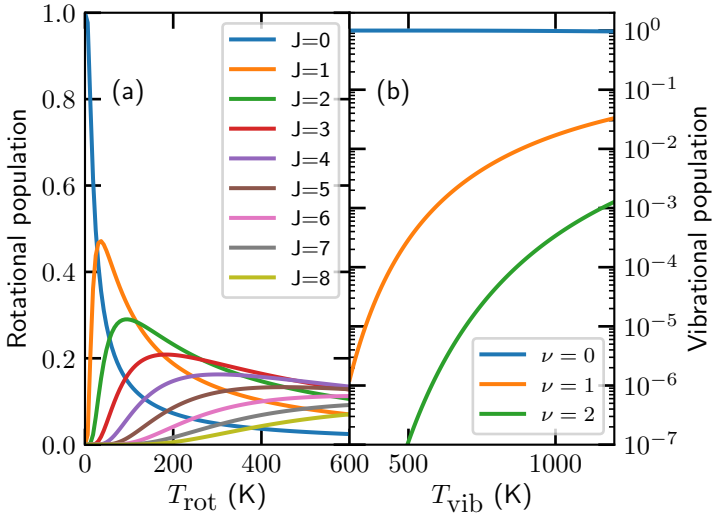

FIGURE 4.5: Rotational (a) and vibrational (b) state populations of HCl according to a Boltzmann distribution as a function of temperature. The rovibrational energies are obtained from the PES.

off-normally (blue squares) incident HCl. Interestingly, it seems that the agreement between theory (solid lines and filled symbols) and experiment (dashed lines and open symbols) is better for off-normally than normally incident HCl. The difference in the sticking probability between the two experimental data sets has previously been explained from the difference in vibrational temperature[49]. Whether this analysis is correct may be gleaned from Figures 4.4c,d, which compares results of calculations for normal incidence and one and the same rotational temperature, but different vibrational temperatures, i.e., $T_{\mathrm{vib}} = 0\,\mathrm{K}$ (orange diamonds) and $T_{\mathrm{vib}} = 1060\,\mathrm{K}$ (blue diamonds). No difference between the computed reaction probabilities is visible using a linear scale (panel c), while a difference is only visible with the use of a logarithmic scale (panel d) if the incidence energy is lower than the minimum barrier in the PES, i.e., 100 kJ/mol. The reason is that, even though the vibrational efficacy for sticking ($\chi_{\nu=1} = 2 - 3$) is high for the energies shown, only two percent of the molecules is vibrationally pre-excited (to $\nu = 1$) at $T_{\mathrm{vib}} = 1060\,\mathrm{K}$ (see Figure 4.5), which is the highest vibrational temperature used in the experiments. Thus, the difference between the normal and off-normal incidence data sets cannot be attributed to the difference in vibrational temperature only.

It has been suggested that the translational energy parallel to the metal

surface might increase the sticking probability as well[60], i.e., the assumption of NES might break down. However, here we do not observe an influence of motion parallel to the surface on the sticking probability (see also Figures 4.D.1g,h). Furthermore, Figures 4.4e,f compare sticking of normally incident HCl with the rotational state distribution either being completely in $J = 0$ (green) or according to a Boltzmann distribution at the maximum rotational temperature achieved in the experiments (orange). Here, we see that also the rotational temperature influences the sticking probability. From Figure 4.4 we conclude that the difference between the sticking probabilities measured for normal and off-normal incidence (presented in Ref. [49], Chapter 3, and the present chapter) are for a large part due to rotational effects. These rotational effects (see also Figure 4.D.1 and Section 4.D) prevent the direct determination of vibrational effects from the experiments discussed, as the vibrational effects are much weaker than the rotational effects over most of the incidence energy range probed.

4.3 Conclusion

In this chapter, a large effect of rotational excitation is found for the dissociative chemisorption of HCl on Au(111). This rotational effect is the cause for a considerable difference in the sticking probability between two experimental data sets, which was previously attributed to vibrational excitation instead. The predicted rotational efficacy can be as large as 20; i.e., rotational energy is much more efficient at promoting the reaction than translational energy. To the best of our knowledge a rotational efficacy this large, or even larger than one, has not been observed so far. Furthermore, pre-exciting both rotation and vibration has a mutually reinforcing effect: The rotational efficacy is increased considerably (from a factor of about 4 to a factor 20). Moreover, the high rotational efficacy is not due to a steering effect, but a lock-in effect where only specific initial rotational phases (i.e., combinations of the polar angle θ and its conjugate momentum) are reactive, which is caused by a non-monotonic dependence of the reaction path on the polar angle θ in the region just in front of the minimum barrier. As a result, the reaction of HCl in the rotational ground state on Au(111) is inefficient, in contrast to that of rotationally pre-excited HCl.

Appendix

4.A Definition of the Sticking Probability

Here, we define the sticking probability as

$$S_0(\langle E_\mathrm{i}(v_0,\alpha)\rangle, T_\mathrm{N}, \Theta_\mathrm{i}) = S_0(\langle E_\mathrm{i}\rangle, T_\mathrm{N}, \Theta_\mathrm{i}) = S_0(E_\mathrm{i}, T_\mathrm{N}, \Theta_\mathrm{i}), \tag{4.4}$$

where T_N is the nozzle temperature and Θ_i the incidence angle. We usually drop the dependence of the average incidence energy $\langle E_\mathrm{i}(v_0,\alpha)\rangle$ on the molecular beam parameters defining the velocity distribution (i.e., the stream velocity v_0 and velocity width α) and write it simply like $\langle E_\mathrm{i}\rangle$. In writing the sticking probability like $S_0(E_\mathrm{i}, T_\mathrm{N}, \Theta_\mathrm{i})$ we tacitly assume that the reader knows that E_i is in fact equal to $\langle E_\mathrm{i}\rangle$. If we consider normal incidence ($\Theta_\mathrm{i} = 0$), we may also drop the incidence angle from the expression and write the sticking probability like $S_0(E_\mathrm{n}, T_\mathrm{N}) = S_0(E_\mathrm{i}, T_\mathrm{N})$, where E_n is the normal incidence energy and in writing this equation we have again tacitly assumed that in fact it is the average normal incidence energy, i.e., $E_\mathrm{n} = \langle E_\mathrm{n}\rangle$. Here,

$$E_\mathrm{n} = \cos^2(\Theta_\mathrm{i}) E_\mathrm{i}. \tag{4.5}$$

If normal energy scaling (NES) holds, we then may simply substitute $S_0(E_\mathrm{n}, T_\mathrm{N})$ for $S_0(E_\mathrm{i}, T_\mathrm{N}, \Theta_\mathrm{i})$.

We also define the initial-state selected reaction probability $R_{\nu,J}(E_\mathrm{i}, \Theta_\mathrm{i})$, where ν and J are the initial vibrational and rotational quantum numbers, respectively. Of course, if we decide to only consider normal incidence, we may also write this as $R_{\nu,J}(E_\mathrm{n})$ or as $R_{\nu,J}(E_\mathrm{i})$, as long as we remember that we are considering normal incidence. And, if we assume NES, we may substitute $R_{\nu,J}(E_\mathrm{n})$ for $R_{\nu,J}(E_\mathrm{i}, \Theta_\mathrm{i})$. Which assumption is made (normal incidence only, or NES holds) has to be clearly stated and we make a decision on this when we present this in this chapter. Here, the symbol R is used instead of $S_0(E_\mathrm{i}, T_\mathrm{N}, \Theta_\mathrm{i})$ to clearly distinguish between an initial-state selected reaction probability that can usually not be directly measured in a molecular beam experiment and the sticking probability, which can be directly measured, but represents an

average over the distribution of incidence energies and of the rovibrational states of the molecules in the incident beam.

4.B Determination of Effective Barrier Heights and Concomitant Vibrational Efficacy

An effective barrier height indicates the incidence energy at which $S_0 = 1/2 S_0^{\max}$, and is typically a parameter in error function fits to experimental sticking probabilities[31, 49, 61]. Previously, the following vibrational state specific S-shaped sticking curves were employed for HCl + Au(111)[49]:

$$S_0^{v=i}(E) = \frac{A_i}{2}\left[1 + \mathrm{erf}\left(\frac{E - E_{0,i}}{W_i}\right)\right], \tag{4.6}$$

where A_i is the saturation value (i.e., $S_0^{\max}$), $E_{0,i}$ is the effective barrier height, W_i is a broadening parameter, and i indicates the vibrational state. Furthermore, it is assumed that only $v = 0$ and $v = 1$ HCl are present in the molecular beam. The constraints employed in the original fitting procedure[49] are $A_0 = A_1 = 1$ and $W_0 = W_1$, whereas for the newly determined lower and upper limits (see Ref. [25]) the constraint of $W_0 = W_1$ is lifted. The parameters of the fitted curves are provided in Table 4.B.1. However, in this approach the role of rotational excitation is assumed to be negligible, which we have shown to be incorrect. For example, neglecting rotational excitation in making the fit, even if the sticking probability of vibrationally excited HCl is unity ($S_0^{v=1}(E_\mathrm{i}) = 1$), the difference between the measured normal and off-normal incidence sticking probabilities is larger than the maximum contribution of the vibrationally excited molecules in the beam (i.e., 0.02, which would be the population of $v = 1$ HCl at $T_\mathrm{N} = 1060\,\mathrm{K}$, see Figures 4.4a,b and 4.5b). Moreover, the agreement between the fitted curves and the experimental data is poor (see Figure 4.B.1). Additionally, E_0 parameters determined for energies larger than the employed normal incidence energy (i.e., $E_0 \geq 299\,\mathrm{kJ/mol}$ (Table 4.B.1), whereas $E_\mathrm{n} \leq 247\,\mathrm{kJ/mol}$ (Tables 4.D.1 and 4.D.2)) may be expected to be inaccurate.

Rotational and vibrational efficacies are often obtained from the aforementioned effective barrier heights as follows (see also Eq. 4.3 and the discussion thereof)[30, 31]:

$$\chi_J(v) = \frac{E_0(v, J = 0) - E_0(v, J)}{E_\mathrm{rot}(v, J) - E_\mathrm{rot}(v, J = 0)}, \tag{4.7}$$

TABLE 4.B.1: Parameters for the S-shaped curves shown in Figure 4.B.1 fitted to the original[49] and newly determined experimental sticking probabilities for $\nu = 0$ and 1 HCl. $E_{0,\nu}$ and W_ν are in kJ/mol, whereas A_ν is unitless.

Results	$E_{0,0}$	W_0	A_0	$E_{0,1}$	W_1	A_1
Old	385.9	48.2	1.0	164.0	48.2	1.0
New (lower limit)	395.6	106.1	1.0	115.8	9.6	1.0
New (upper limit)	299.1	77.2	1.0	96.5	19.3	1.0

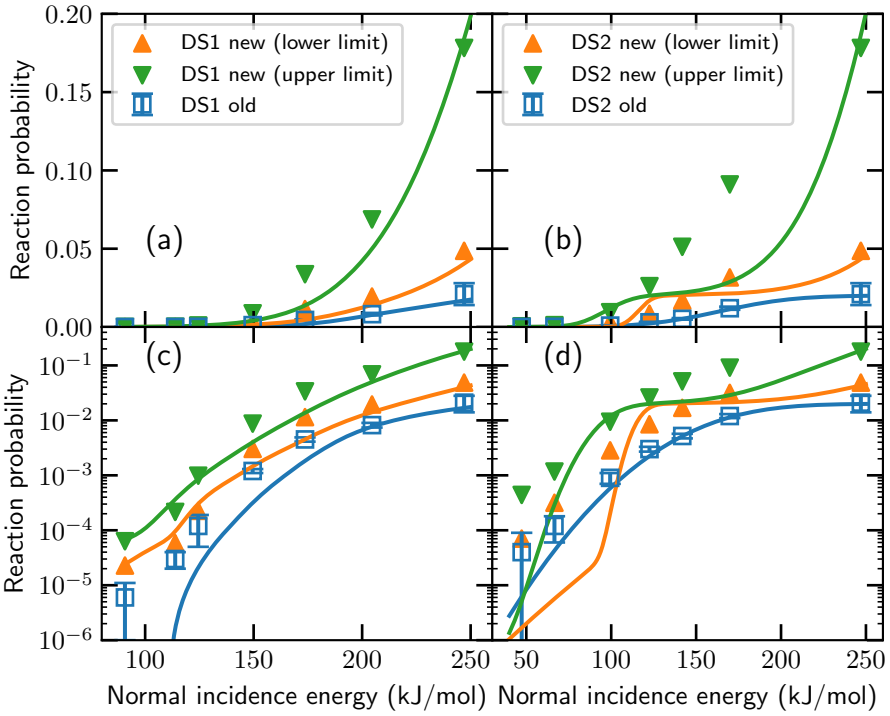

FIGURE 4.B.1: Experimental sticking probabilities of HCl on Au(111) for normally (DS1; a,c) and off-normally (DS2; b,d) incident HCl, where DS1 and DS2 refer to the employed beam parameters (see text). The blue diamonds indicate the original experimental results[49], whereas the orange upwards facing (green downwards facing) triangles indicate the newly determined lower (upper) limit (see Chapter 3). The solid lines are the error function fits to the data discussed in Section 4.B. Panels c and d are identical to panels a and b, respectively, except that a logarithmic scale is used instead.

$$\chi_\nu(J) = \frac{E_0(\nu=0,J) - E_0(\nu,J)}{E_{\text{vib}}(\nu,J) - E_{\text{vib}}(\nu=0,J)}. \tag{4.8}$$

The vibrational efficacies are 6.4, 8.1 and 5.9 for the original, and newly determined lower and upper limit E_0 parameters, respectively. This is clearly much too large when compared to our calculations (see Table 4.1). At the same time, this approach does not take into account the R dependence of the efficacy, which we also consider to be a too severe approximation since efficacies can vary wildly with R (see Figure 4.1 and Table 4.1). In conclusion, an analysis of the experimental results based on the assumption of a rotational efficacy of 0, and in terms of vibrational effects only, is too simple and will lead to overestimated vibrational efficacies.

4.C Experimental State-Specific Sticking Probabilities

For the predicted laser-on sticking probabilities shown in Figure 4.4, several experimental limitations are taken into account. First, in the molecular beam two HCl isotopes, i.e., ^{35}HCl and ^{37}HCl, would usually be present, of which only one can be excited due to the mass mismatch between the two isotopes and concomitant frequency shift. As such, in the simulated laser-on results only $3/4^{\text{th}}$ of the molecules (the fraction of ^{35}HCl in an HCl gas) in the targeted rovibrational state can be excited.

An excitation efficiency of close to 100%, which can be achieved for some molecules by rapid adiabatic passage (RAP)[14, 62–65], cannot be achieved with RAP for HCl. The reason is that the narrow frequency bandwidth of the laser that would be required for RAP would make it impossible to transfer all of the population in the ($\nu = 0, J$) to the upper ($\nu = 1$ or 2, J') state: The energy ranges spanned between the fine structure states associated with the nuclear spin of Cl and J in both the upper and lower levels exceed the required laser band width by too much to achieve a laser excitation efficiency greater than 50%[66–68]. Thus, only $3/4 \times 1/2 = 3/8^{\text{th}}$ of the molecules initially in a specific (ν, J) state can be excited. Furthermore, the selection rules for the R branch ($\nu = 0, J$ to $\nu' = 1$ or 2, $J' = J + 1$) and P branch ($\nu = 0, J$ to $\nu' = 1$ or 2, $J' = J - 1$) excitations are taken into account.

Experiments using laser excitation would measure both a "laser-off" and a "laser-on" sticking probability, where the latter can be written as

$$S_0^{\text{laser-on}}(E_i) = S_0^{\text{laser-off}}(E_i) + f_{\text{exc}}\left(S_0^{v',J'}(E_i) - S_0^{v,J=J'\pm1}(E_i)\right) \tag{4.9}$$

if excitation takes place from the (ν, J) to the (ν', J') state, and if the fraction of HCl molecules transferred between these states, f_{exc}, is given by

$$f_{\mathrm{exc}} = f_{\mathrm{sat}} f_{\nu}(T_{\mathrm{vib}}) f_{J}(T_{\mathrm{rot}}). \tag{4.10}$$

Here, f_{sat} is equal to 3/8, as already established above. The product $f_{\nu}(T_{\mathrm{vib}}) \times f_{J}(T_{\mathrm{rot}})$ yields a Boltzmann-like population of the (ν, J) state excited from in the molecular beam, where we take into account that the rotational and vibrational temperatures of the molecules in the beam may differ, assume that these can be related to the nozzle temperature in some way (see Tables 4.D.1 and 4.D.2 for their values), and have made the approximation that the rotational constants of the molecule are independent of the vibrational state. Obviously, the initial-state selected reaction probability $S_0^{v',J'}(E_{\mathrm{i}})$ that we are after can be calculated from Eqs. 4.9 and 4.10 using the equation also used when extracting these probabilities from experiments, i.e.,

$$S_0^{\nu',J'}(E_{\mathrm{i}}) = \frac{S_0^{\text{laser-on}}(E_{\mathrm{i}}) - S_0^{\text{laser-off}}(E_{\mathrm{i}})}{f_{\mathrm{exc}}} + S_0^{\nu=0,J=J'\pm1}(E_{\mathrm{i}}). \tag{4.11}$$

As can be seen from Eq. 4.11, it will be possible to extract accurate values of $S_0^{v',J'}(E_{\mathrm{i}})$ from experiments if the difference between the laser-on and laser-off sticking probabilities is sufficiently large (as addressed by Figures 4.2b,c) in comparison to the error bars with which these quantities are measured (this is not addressed in Figure 4.2), and if $S_0^{v,J=J'\pm1}(E_{\mathrm{i}})$ is either known in advance, or can be assumed to be zero or approximately equal to the laser-off sticking probability. Of course, in calculations we do not have this difficulty and in the simulation of the experiment we can simply use a calculated value for $S_0^{v,J=J'\pm1}(E_{\mathrm{i}})$. Another way to obtain $S_0^{\nu=0,J=J'\pm1}$ is to employ the ratio of $S_0^{\nu=0,J=J'\pm1}/S_0^{\text{laser-off}}$ from simulations[17], although this might require a PES that is in better quantitative agreement with the experimental sticking probabilities than employed in this chapter. Here, however, the problem is solved by simply using the calculated $S_0^{\text{laser-off}}$, $S_0^{\nu=0,J=J'\pm1}$ and $S_0^{v',J'}(E_{\mathrm{i}})$ to predict $S_0^{\text{laser-on}}(E_{\mathrm{i}})$.

4.D The Two Experimental Data Sets and the Origin of Their Differences

Specifically, the main differences between the experiments yielding the DS1 and the DS2 datasets are as follows[49]. The DS1 experiments were per-

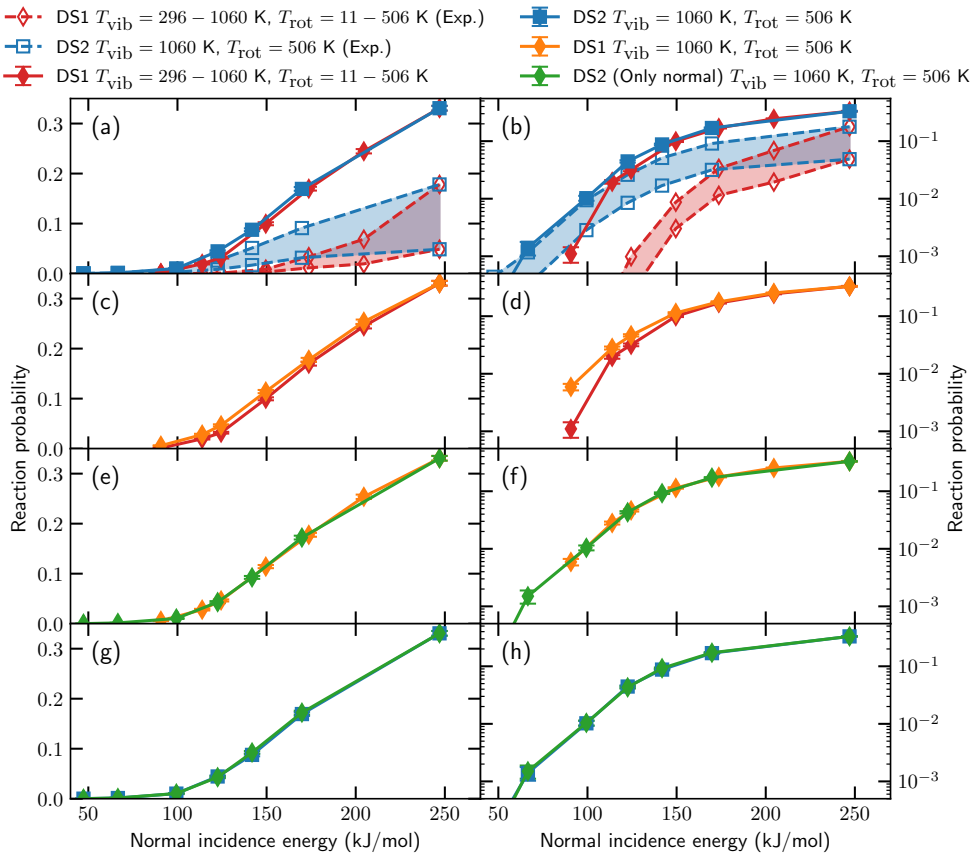

FIGURE 4.D.1: Sticking probability of HCl on Au(111) as a function of normal incidence energy for various conditions ((off-)normal indicidence, and vibrational and rotational temperatures). The open symbols and dashed lines indicate experimental results, where the shaded area indicates their uncertainty. The solid symbols and lines indicate computed results. The diamonds (squares) are for (off-)normal incidence, where the color indicates the rotational and vibrational temperatures (see legend). DS1 and DS2 refer to the employed beam parameters (see text in Section 4.D). The error bars represent 68% confidence intervals. Panels b, d, f and h are identical to panels a, c, e, and g, respectively, except that a logarithmic scale is used instead. For further details see Section 4.D.

formed for normal incidence, and the (normal) incidence energy was varied by changing the nozzle temperature, so that the normal incidence energy on the one hand and the vibrational and rotational temperatures on the other hand were not varied independently in these experiments. In contrast, the DS2 experiments were performed while keeping the nozzle temperature (and therefore T_{vib} and T_{rot}) constant, while varying the normal incidence energy by varying the incidence angle and the seeding gas mixture. Therefore, in these experiments the normal incidence energy could be varied independently from the rovibrational state populations; however, in the DS2 case there is parallel translational energy present, and this varies with the normal incidence angle. As can be seen from Figures 4.D.1a,b, for similar normal incidence energy the computed DS2 sticking probabilities are higher than the computed DS1 sticking probabilities. The same is true for the measured values as first published[49], but also for the upper and lower bounds to these probabilities obtained by reanalyzing the data (Figures 4.D.1a,b)[25, 69].

With the "experimental knobs" that can be turned to change conditions between the two experiments yielding sticking probabilities as functions of normal incidence energy, one cannot vary all quantities determining these sticking probabilities independently, as discussed above. Of course in theory, one can, as discussed already to some extent in the discussion of Figure 4.4. Here, we enter into additional details. In the first step going from the DS1 to the DS2 conditions, i.e., in turning the first "computational knob" to stay with our previous analogy, we keep all conditions in the DS1 experiment the same, except that we now adopt the same T_{vib} and T_{rot} temperature as used in all the DS2 experiments. We keep the beam parameters describing the velocity distributions in the DS1 experiments the same, and perform the simulations for normal incidence. Figures 4.D.1c,d then show the effect of changing to DS2 conditions for T_{vib} and T_{rot} while keeping all other conditions the same as in the DS1 experiments. Here, we see that the sticking probability increases with the rovibrational temperature. As discussed in Section 4.2.3, this increase is mostly caused by the increase in rotational temperature, and not by the increase in vibrational temperature (see also Figures 4.4c,d,g,h). Only for incidence energies below the barrier height does the vibrational temperature have a considerable effect on the sticking probability (Figure 4.4d).

The second step is to additionally employ the beam parameters describing the velocity distributions of DS2 (green) instead of DS1 (orange, see Figures 4.D.1e,f), but without including the effect of changing the incidence angle (i.e., the translational energy parallel to the surface remains zero). No considerable changes are observed and therefore we conclude that the change in stream velocity and width when going from DS1 to DS2 does not influence the sticking

TABLE 4.D.1: Beam parameters from Ref. [49] that describe the simulated HCl velocity distributions of data set 1 (DS1). The stream energy E_0, stream velocity v_0, and velocity width parameter α have been determined through time-of-flight measurements. The incidence angle is normal to the surface.

$T_{N,vib}$ (K)	T_{rot} (K)	$\langle E_i \rangle$ (kJ/mol)	E_0 (kJ/mol)	v_0 (m/s)	α (m/s)
296	11	91	90	2219	158
400	78	114	110	2456	245
500	143	124	120	2562	207
620	221	150	144	2808	292
740	298	174	167	3026	323
910	409	205	196	3278	364
1060	506	247	238	3616	371

TABLE 4.D.2: Beam parameters from Ref. [49] that describe the simulated HCl velocity distributions of data set 2 (DS2). The stream energy E_0, stream velocity v_0, and velocity width parameter α have been determined through time-of-flight measurements. The nozzle temperature is 1060 K, yielding $T_{vib} = 1060$ K and $T_{rot} = 506$ K.

$\langle E_i \rangle$ (kJ/mol)	$\langle E_\perp \rangle$ (kJ/mol)	$\langle E_\parallel \rangle$ (kJ/mol)	Θ_i (°)	E_0 (kJ/mol)	v_0 (m/s)	α (m/s)
114	47	67	50	114	2500	273
114	67	47	40	114	2500	273
241	99	142	50	234	3586	321
236	123	114	44	230	3549	322
241	142	99	40	234	3586	321
236	170	67	32	230	3549	322
247	247	0	0	238	3616	371

probability considerably.

The final step is to also include the translational energy parallel to the surface (Figures 4.D.1g,h), which is present due to an off-normal incidence angle, thus completely employing the DS2 conditions (blue). Similar to the beam parameters, including parallel translational energy does not influence the sticking probability considerably.

In summary, the difference between the DS1 and DS2 sticking probabilities is caused mainly by the rotational temperature, whereas the vibrational temperature only has an effect for incidence energies below the barrier height, and the stream velocity and width, and motion parallel to the surface have no visible effect on the sticking probability.

4.E The Mechanism Underlying the High Rotational Efficacy

The distributions of the θ angle of reacting HCl are shown for several HCl bond lengths and rovibrational states in Figure 4.E.1. Similarly, Figure 4.E.2 shows the distribution of the θ angle along the reaction coordinate. The reaction coordinate S is defined here through the change in Z_{HCl} and r_{HCl} along the MEP or during a trajectory:

$$S = \Delta Z_{\mathrm{HCl}} + \Delta r_{\mathrm{HCl}}, \tag{4.12}$$

where at the TS $S = 0$. Although generally the reaction coordinate is taken to be mass weighted, here, the masses are neglected due to the small dependence of the reaction coordinate on r. Additionally, movement of the center of mass in the XY plane is neglected, since little movement in the XY plane is observed in normally incident HCl MD simulations (see Chapter 3). In general, the initial θ distributions are broad and become more narrow when the bond is extended, eventually moving the distributions close to the minimum TS value ($\theta = 117°$) (Figures 4.E.1 and 4.E.2). At lower r values, increasing the rotational energy ($J = 2 \rightarrow 8$) increases the width of the θ distribution, making low initial θ values more reactive (Figure 4.E.1a). Similarly, increasing the vibrational energy ($\nu = 0 \rightarrow 2$) increases the width of the initial θ distribution as well (Figure 4.E.1b). This effect is also observed in Figure 4.E.3, where S_0 is shown as a function of θ. Furthermore, when the vibrational energy is increased, the focusing of the distribution towards the TS value occurs at a larger r value (compare Figures 4.E.1e,f and Figures 4.E.1g,h).

Figures 4.E.4, 4.E.5 and 4.E.6 show the relative reactivity of combinations of the initial values of θ and its conjugate momentum compared to its statistical distribution in the simulated molecular beams. Interestingly, the reactivity depends on the combination of the orientation and angular momentum (i.e., the rotational phase), and is also rotational state specific. Furthermore, the results suggest that since the higher J states allow for more different orientations and angular momenta, the molecule is perhaps more easily focused towards a reactive pathway if it is in a high J state.

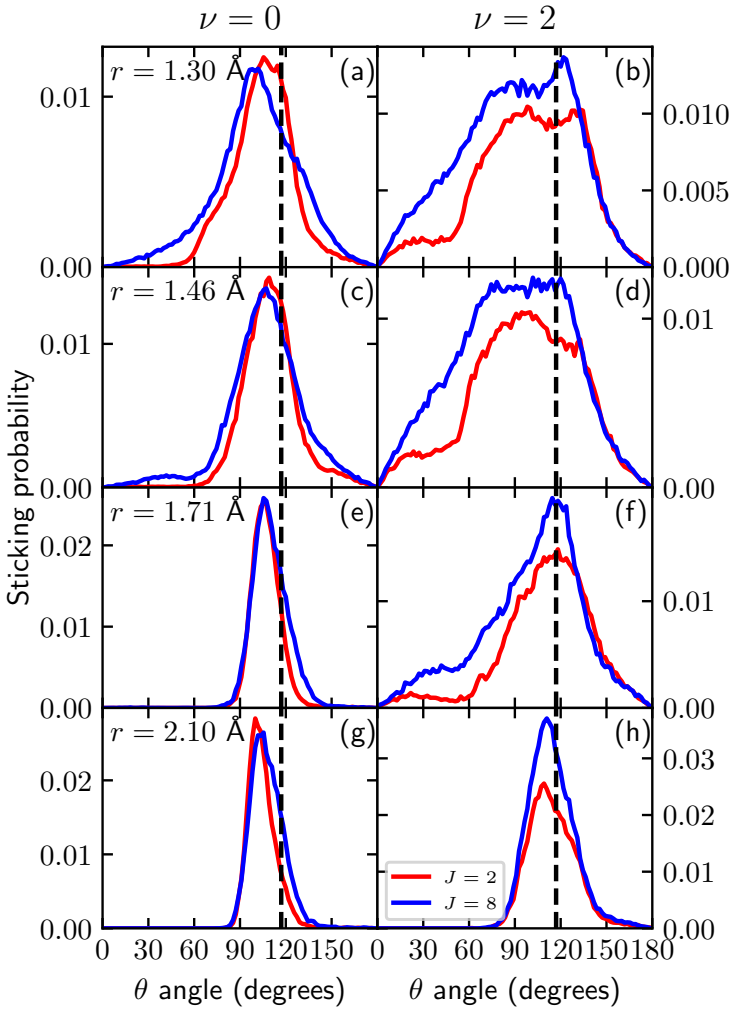

FIGURE 4.E.1: Distribution of the θ angle of reacting HCl on Au(111) for several bond lengths. Red and blue indicate $J = 2$ and 8, respectively. The left panels are for $\nu = 0$ and the right panels are for $\nu = 2$. The average normal indicidence energy is 247 kJ/mol. For the analysis of the trajectories only $Z_{Cl} < 2.5$ Å is considered. The black dashed line indicates the minimum TS value.

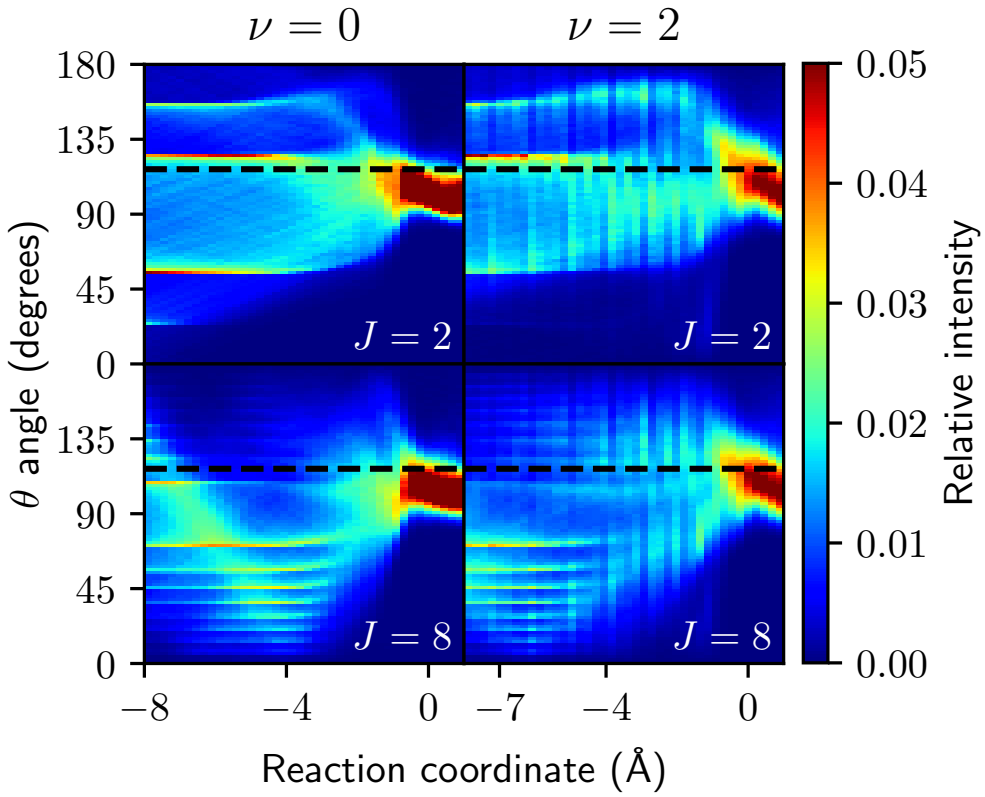

FIGURE 4.E.2: Distribution of the θ angle of reacting HCl on Au(111) along the reaction path. The average normal indicidence energy is 247 kJ/mol, $\nu = 0$ or 2 (left and right panels, respectively), and $J = 2$ or 8 (top and bottom panels, respectively). The black dashed line indicates the minimum TS value.

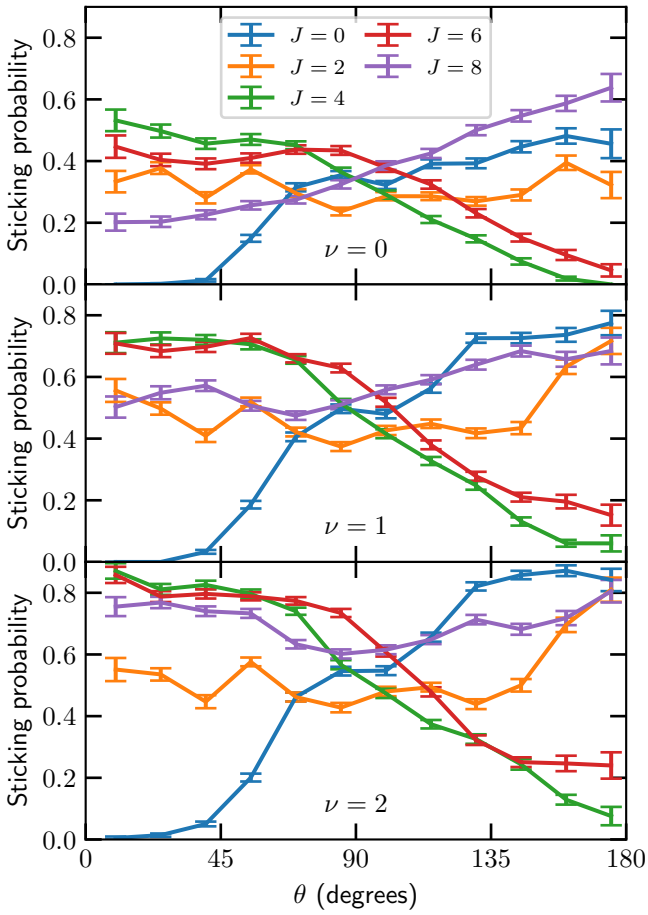

FIGURE 4.E.3: Sticking probability as a function of the initial θ angle of HCl on Au(111) for $\langle E_i \rangle = 247\,\mathrm{kJ/mol}$. Results for several rovibrational states are shown, as indicated in the legend of the upper panel. The error bars represent 68% confidence intervals.

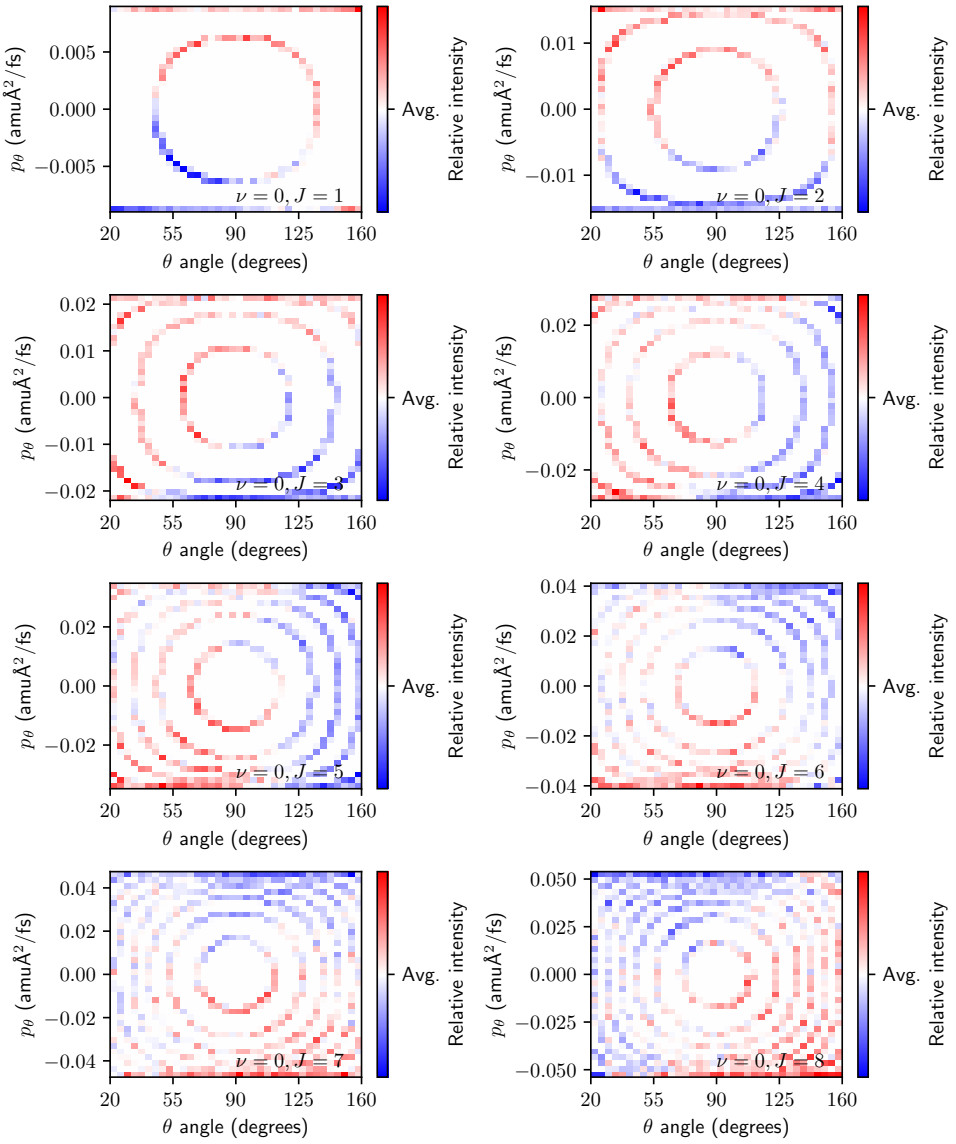

FIGURE 4.E.4: Distribution of the initial θ angle and its conjugate momentum of reacting HCl on Au(111) for $\nu = 0$ and $J = 1 - 8$. The colors indicate the intensity of reactive combinations of θ and p_θ relative to the statistical distribution in the simulated molecular beam; i.e., blue indicates that the combination is less reactive compared to its statistical occurrence whereas red indicates a relatively higher reactivity. The data have been normalized along the θ angle to remove the $\sin\theta$ distribution in the initial statistical distribution, i.e., with the renormalization performed all initial θ angles have equal probability.

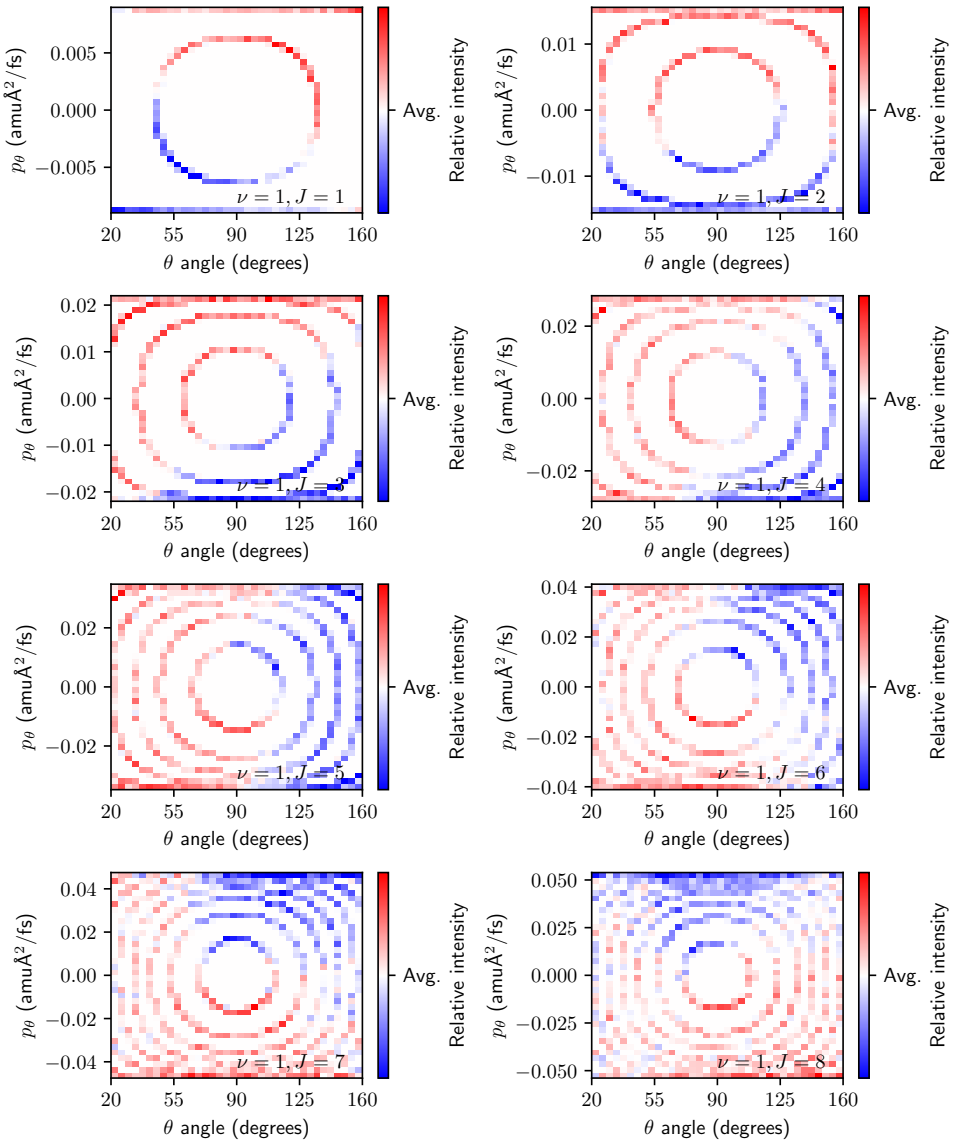

FIGURE 4.E.5: Same as Figure 4.E.4 but for $\nu = 1$.

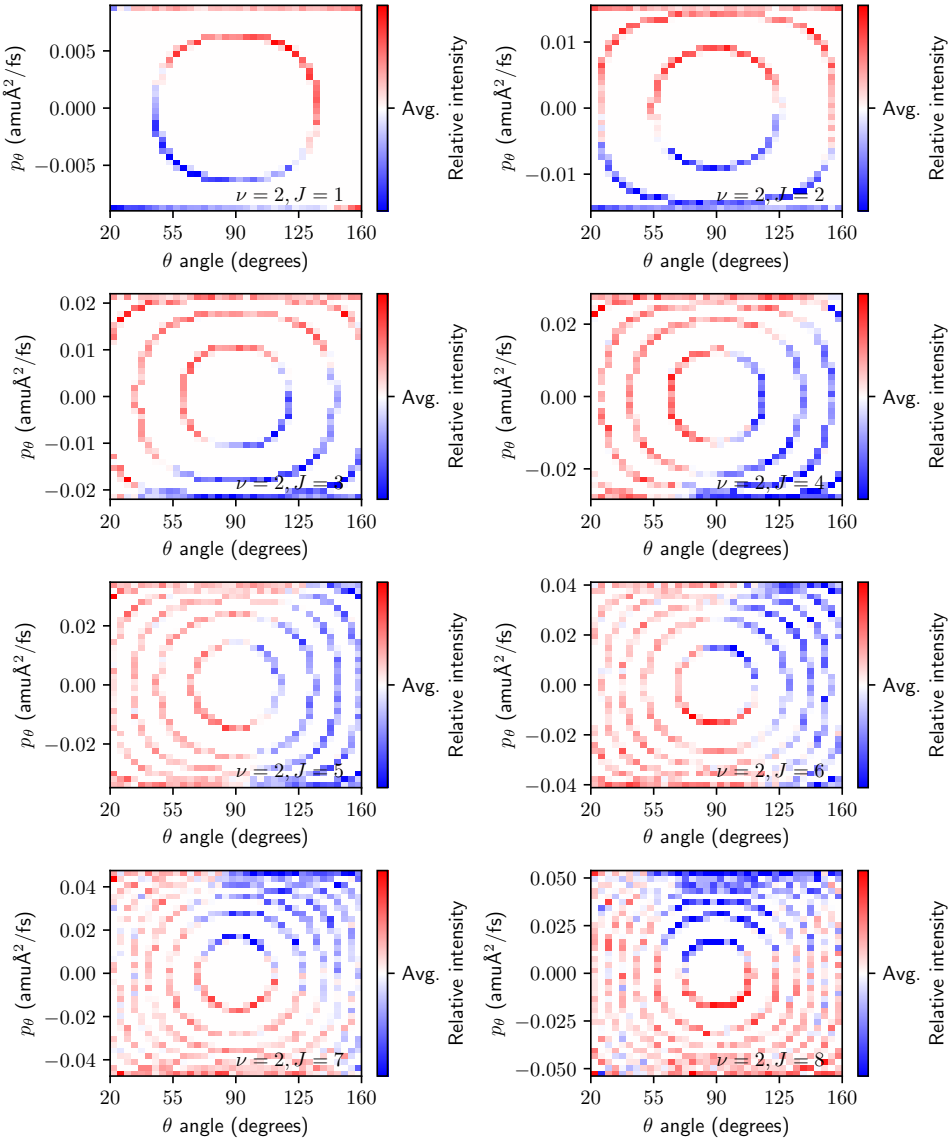

FIGURE 4.E.6: Same as Figure 4.E.4 but for $\nu = 2$.

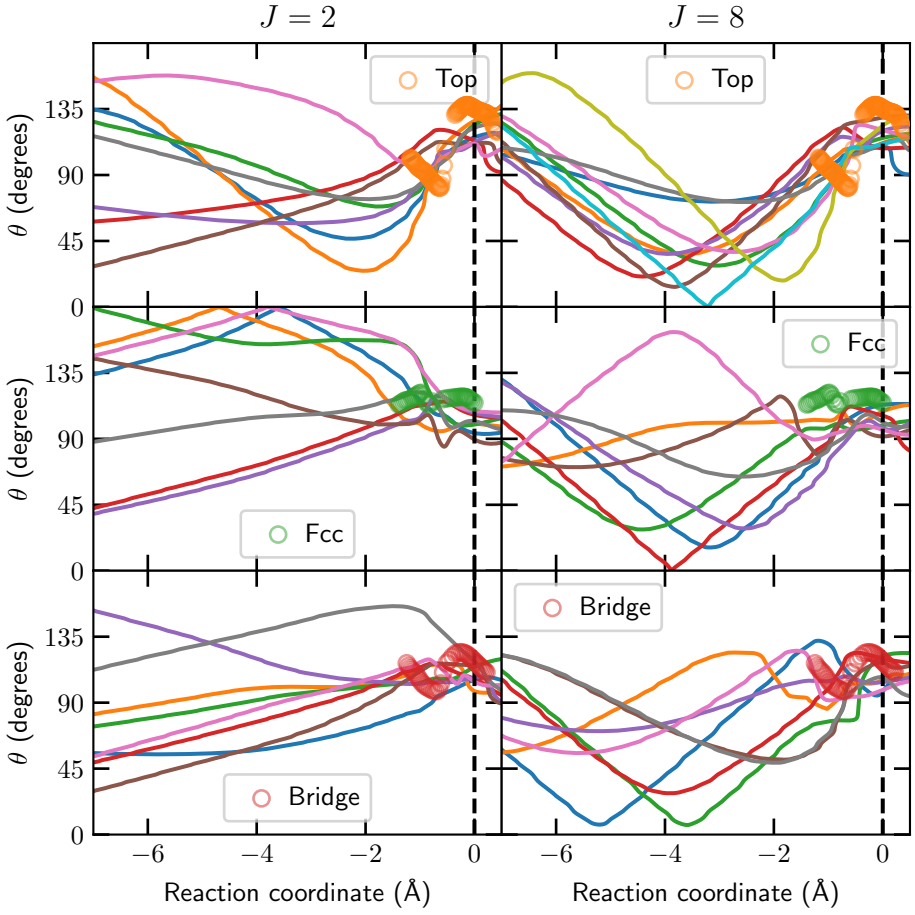

FIGURE 4.E.7: θ angle along the reaction path for a few representative trajectories reacting at the top, fcc, and bridge sites for $v = 0$ and $J = 2$ (left panels) or 8 (right panels). The θ angle along the MEP for the top, fcc, and bridge sites is indicated by the orange, green, and red circles, respectively. The dashed line indicates the location of the reaction barrier, i.e., $r = r^{\ddagger}$.

4.F Synergistic Effect of Rotational and Vibrational Pre-excitation

Rotational and vibrational pre-excitation of HCl has a synergistic effect on S_0, which we will discuss now. The initial distribution of the θ angle is broad for all rovibrational states considered, whereas at the moment of reaction (i.e., $r = r^{\ddagger} = 2.18$ Å) the distribution is more narrow and nearer the TS value (see Figures 4.E.1 and 4.E.2). Both rotational and vibrational pre-excitation cause a broader initial θ distribution to be reactive (Figures 4.E.1a,b). Furthermore, rotational reorientation is required due to large changes in the optimum value along the MEP and due to a narrow bottleneck in θ leading up to the dissociation (see Section 4.2.2). On the other hand, vibrational excitation causes the bottleneck to occur later along the reaction path, while the rotational reorientation occurs in a shorter timeframe (see especially Figure 4.E.1). It is possible that this shortening of the reorientation timeframe causes rotational excitation to have an even larger effect on S_0. In any case, we see that pre-exciting rotation and vibration simultaneously has a mutually reinforcing effect on the sticking probability.

References

(1) Sorgenti, H. A.; Sachsel, G. F. Nitric Acid Manufacture—Theory and Practice. *Ind. Eng. Chem.* **1960**, *52*, 101–104, DOI: 10.1021/ie50602a019.

(2) Ertl, G. Primary Steps in Catalytic Synthesis of Ammonia. *J. Vac. Sci. Technol. A* **1983**, *1*, 1247–1253, DOI: 10.1116/1.572299.

(3) Rostrup-Nielsen, J. R.; Sehested, J.; Nørskov, J. K. In *Advances in Catalysis*; Academic Press: 2002; Vol. 47, pp 65–139, DOI: 10.1016/S0360-0564(02)47006-X.

(4) Sá, S.; Silva, H.; Brandão, L.; Sousa, J. M.; Mendes, A. Catalysts for Methanol Steam Reforming—A Review. *Appl. Catal. B* **2010**, *99*, 43–57, DOI: 10.1016/j.apcatb.2010.06.015.

(5) Fisch, A. G. In *Kirk-Othmer Encyclopedia of Chemical Technology*; John Wiley & Sons: 2019, pp 1–22, DOI: 10.1002/0471238961.2609050703050303.a01.pub2.

(6) Wolcott, C. A.; Medford, A. J.; Studt, F.; Campbell, C. T. Degree of Rate Control Approach to Computational Catalyst Screening. *J. Catal.* **2015**, *330*, 197–207, DOI: 10.1016/j.jcat.2015.07.015.

(7) Ertl, G. Elementary Steps in Heterogeneous Catalysis. *Angew. Chem. Int. Ed.* **1990**, *29*, 1219–1227, DOI: 10.1002/anie.199012191.

(8) Sabbe, M. K.; Reyniers, M.-F.; Reuter, K. First-Principles Kinetic Modeling in Heterogeneous Catalysis: An Industrial Perspective on Best-Practice, Gaps and Needs. *Catal. Sci. Technol.* **2012**, *2*, 2010–2024, DOI: 10.1039/C2CY20261A.

(9) Juurlink, L. B. F.; McCabe, P. R.; Smith, R. R.; DiCologero, C. L.; Utz, A. L. Eigenstate-Resolved Studies of Gas-Surface Reactivity: CH_4 ν_3 Dissociation on Ni(100). *Phys. Rev. Lett.* **1999**, *83*, 868–871, DOI: 10.1103/PhysRevLett.83.868.

(10) Smith, R. R.; Killelea, D. R.; DelSesto, D. F.; Utz, A. L. Preference for Vibrational over Translational Energy in a Gas-Surface Reaction. *Science* **2004**, *304*, 992–995, DOI: 10.1126/science.1096309.

(11) Killelea, D. R.; Campbell, V. L.; Shuman, N. S.; Utz, A. L. Bond-Selective Control of a Heterogeneously Catalyzed Reaction. *Science* **2008**, *319*, 790–793, DOI: 10.1126/science.1152819.

(12) Juurlink, L. B. F.; Killelea, D. R.; Utz, A. L. State-Resolved Probes of Methane Dissociation Dynamics. *Prog. Surf. Sci.* **2009**, *84*, 69–134, DOI: 10.1016/j.progsurf.2009.01.001.

(13) Shen, X. J.; Lozano, A.; Dong, W.; Busnengo, H. F.; Yan, X. H. Towards Bond Selective Chemistry from First Principles: Methane on Metal Surfaces. *Phys. Rev. Lett.* **2014**, *112*, 046101, DOI: 10.1103/PhysRevLett.112.046101.

(14) Hundt, P. M.; Ueta, H.; van Reijzen, M. E.; Jiang, B.; Guo, H.; Beck, R. D. Bond-Selective and Mode-Specific Dissociation of CH_3D and CH_2D_2 on Pt(111). *J. Phys. Chem. A* **2015**, *119*, 12442–12448, DOI: 10.1021/acs.jpca.5b07949.

(15) Jiang, B.; Guo, H. Dynamics of Water Dissociative Chemisorption on Ni(111): Effects of Impact Sites and Incident Angles. *Phys. Rev. Lett.* **2015**, *114*, 166101, DOI: 10.1103/PhysRevLett.114.166101.

(16) Zhang, Z.; Liu, T.; Fu, B.; Yang, X.; Zhang, D. H. First-Principles Quantum Dynamical Theory for the Dissociative Chemisorption of H_2O on Rigid Cu(111). *Nat. Commun.* **2016**, *7*, 11953, DOI: 10.1038/ncomms11953.

(17) Nattino, F.; Migliorini, D.; Kroes, G.-J.; Dombrowski, E.; High, E. A.; Killelea, D. R.; Utz, A. L. Chemically Accurate Simulation of a Polyatomic Molecule-Metal Surface Reaction. *J. Phys. Chem. Lett.* **2016**, *7*, 2402–2406, DOI: 10.1021/acs.jpclett.6b01022.

(18) Migliorini, D.; Chadwick, H.; Nattino, F.; Gutiérrez-González, A.; Dombrowski, E.; High, E. A.; Guo, H.; Utz, A. L.; Jackson, B.; Beck, R. D.; Kroes, G.-J. Surface Reaction Barriometry: Methane Dissociation on Flat and Stepped Transition-Metal Surfaces. *J. Phys. Chem. Lett.* **2017**, *8*, 4177–4182, DOI: 10.1021/acs.jpclett.7b01905.

(19) Gerrits, N.; Migliorini, D.; Kroes, G.-J. Dissociation of CHD_3 on Cu(111), Cu(211), and Single Atom Alloys of Cu(111). *J. Chem. Phys.* **2018**, *149*, 224701, DOI: 10.1063/1.5053990.

(20) Chadwick, H.; Migliorini, D.; Kroes, G. J. CHD_3 Dissociation on Pt(111): A Comparison of the Reaction Dynamics Based on the PBE Functional and on a Specific Reaction Parameter Functional. *J. Chem. Phys.* **2018**, *149*, 044701, DOI: 10.1063/1.5039458.

(21) Gerrits, N.; Kroes, G.-J. An AIMD Study of Dissociative Chemisorption of Methanol on Cu(111) with Implications for Formaldehyde Formation. *J. Chem. Phys.* **2019**, *150*, 024706, DOI: 10.1063/1.5070129.

(22) Gerrits, N.; Shakouri, K.; Behler, J.; Kroes, G.-J. Accurate Probabilities for Highly Activated Reaction of Polyatomic Molecules on Surfaces Using a High-Dimensional Neural Network Potential: CHD_3 + Cu(111). *J. Phys. Chem. Lett.* **2019**, *10*, 1763–1768, DOI: 10.1021/acs.jpclett.9b00560.

(23) Gerrits, N.; Chadwick, H.; Kroes, G.-J. Dynamical Study of the Dissociative Chemisorption of CHD_3 on Pd(111). *J. Phys. Chem. C* **2019**, *123*, 24013–24023, DOI: 10.1021/acs.jpcc.9b05757.

(24) Gerrits, N.; Kroes, G.-J. Curious Mechanism of the Dissociative Chemisorption of Ammonia on Ru(0001). *J. Phys. Chem. C* **2019**, *123*, 28291–28300, DOI: 10.1021/acs.jpcc.9b09121.

(25) Gerrits, N.; Geweke, J.; Smeets, E. W. F.; Voss, J.; Wodtke, A. M.; Kroes, G.-J. Closing the Gap Between Experiment and Theory: Reactive Scattering of HCl from Au(111). *J. Phys. Chem. C* **2020**, *124*, 15944–15960, DOI: 10.1021/acs.jpcc.0c03756.

(26) Moiraghi, R.; Lozano, A.; Peterson, E.; Utz, A.; Dong, W.; Busnengo, H. F. Nonthermalized Precursor-Mediated Dissociative Chemisorption at High Catalysis Temperatures. *J. Phys. Chem. Lett.* **2020**, *11*, 2211–2218, DOI: 10.1021/acs.jpclett.0c00260.

(27) Jackson, B. Direct and Trapping-Mediated Pathways to Dissociative Chemisorption: CH_4 Dissociation on Ir(111) with Step Defects. *J. Chem. Phys.* **2020**, *153*, 034704, DOI: 10.1063/5.0012252.

(28) Zeng, X.; Qiu, Z.; Li, P.; Li, Z.; Yang, J. Steric Hindrance Effect in High-Temperature Reactions. *CCS Chem.* **2020**, *2*, 460–467, DOI: 10.31635/ccschem.020.202000155.

(29) Rettner, C. T.; DeLouise, L. A.; Auerbach, D. J. Effect of Incidence Kinetic Energy and Surface Coverage on the Dissociative Chemisorption of Oxygen on W(110). *J. Chem. Phys.* **1986**, *85*, 1131–1149, DOI: 10.1063/1.451310.

(30) Michelsen, H. A.; Rettner, C. T.; Auerbach, D. J.; Zare, R. N. Effect of Rotation on the Translational and Vibrational Energy Dependence of the Dissociative Adsorption of D_2 on Cu(111). *J. Chem. Phys.* **1993**, *98*, 8294–8307, DOI: 10.1063/1.464535.

(31) Rettner, C. T.; Michelsen, H. A.; Auerbach, D. J. Quantum-state-specific Dynamics of the Dissociative Adsorption and Associative Desorption of H_2 at a Cu(111) Surface. *J. Chem. Phys.* **1995**, *102*, 4625–4641, DOI: 10.1063/1.469511.

(32) Luntz, A. C.; Brown, J. K.; Williams, M. D. Molecular Beam Studies of H_2 and D_2 Dissociative Chemisorption on Pt(111). *J. Chem. Phys.* **1990**, *93*, 5240–5246, DOI: 10.1063/1.459669.

(33) Chadwick, H.; Guo, H.; Gutiérrez-González, A.; Menzel, J. P.; Jackson, B.; Beck, R. D. Methane Dissociation on the Steps and Terraces of Pt(211) Resolved by Quantum State and Impact Site. *J. Chem. Phys.* **2018**, *148*, 014701, DOI: 10.1063/1.5008567.

(34) Migliorini, D.; Nattino, F.; Tiwari, A. K.; Kroes, G.-J. HOD on Ni(111): Ab Initio Molecular Dynamics Prediction of Molecular Beam Experiments. *J. Chem. Phys.* **2018**, *149*, 244706, DOI: 10.1063/1.5059357.

(35) Chen, J.; Zhou, X.; Zhang, Y.; Jiang, B. Vibrational Control of Selective Bond Cleavage in Dissociative Chemisorption of Methanol on Cu(111). *Nat. Commun.* **2018**, *9*, 4039, DOI: 10.1038/s41467-018-06478-6.

(36) Díaz, C.; Olsen, R. A.; Auerbach, D. J.; Kroes, G. J. Six-Dimensional Dynamics Study of Reactive and Non Reactive Scattering of H_2 from Cu(111) Using a Chemically Accurate Potential Energy Surface. *Phys. Chem. Chem. Phys.* **2010**, *12*, 6499–6519, DOI: 10.1039/C001956A.

(37) Donald, S. B.; Harrison, I. Rice–Ramsperger–Kassel–Marcus Simulation of Hydrogen Dissociation on Cu(111): Addressing Dynamical Biases, Surface Temperature, and Tunneling. *J. Phys. Chem. C* **2014**, *118*, 320–337, DOI: 10.1021/jp408714s.

(38) Xiao, Y.; Dong, W.; Busnengo, H. F. Reactive Force Fields for Surface Chemical Reactions: A Case Study with Hydrogen Dissociation on Pd Surfaces. *J. Chem. Phys.* **2010**, *132*, 014704, DOI: 10.1063/1.3265854.

(39) Chen, J.-C.; Ramos, M.; Arasa, C.; Juanes-Marcos, J. C.; Somers, M. F.; Martínez, A. E.; Díaz, C.; Olsen, R. A.; Kroes, G.-J. Dynamics of H_2 Dissociation on the 1/2 ML c(2x2)-Ti/Al(100) Surface. *Phys. Chem. Chem. Phys.* **2012**, *14*, 3234–3247, DOI: 10.1039/C2CP23693A.

(40) Wijzenbroek, M.; Helstone, D.; Meyer, J.; Kroes, G.-J. Dynamics of H_2 Dissociation on the Close-Packed (111) Surface of the Noblest Metal: H_2 + Au(111). *J. Chem. Phys.* **2016**, *145*, 144701, DOI: 10.1063/1.4964486.

(41) Shuai, Q.; Kaufmann, S.; Auerbach, D. J.; Schwarzer, D.; Wodtke, A. M. Evidence for Electron–Hole Pair Excitation in the Associative Desorption of H_2 and D_2 from Au(111). *J. Phys. Chem. Lett.* **2017**, *8*, 1657–1663, DOI: 10.1021/acs.jpclett.7b00265.

(42) Kaufmann, S.; Shuai, Q.; Auerbach, D. J.; Schwarzer, D.; Wodtke, A. M. Associative Desorption of Hydrogen Isotopologues from Copper Surfaces: Characterization of Two Reaction Mechanisms. *J. Chem. Phys.* **2018**, *148*, 194703, DOI: 10.1063/1.5025666.

(43) Juurlink, L. B.; Smith, R. R.; Utz, A. L. The Role of Rotational Excitation in the Activated Dissociative Chemisorption of Vibrationally Excited Methane on Ni(100). *Faraday Discuss.* **2000**, *117*, 147–160, DOI: 10.1039/B003708G.

(44) Friedrich, B.; Pullman, D. P.; Herschbach, D. R. Alignment and Orientation of Rotationally Cool Molecules. *J. Phys. Chem.* **1991**, *95*, 8118–8129, DOI: 10.1021/j100174a021.

(45) Aquilanti, V.; Ascenzi, D.; Cappelletti, D.; Pirani, F. Velocity Dependence of Collisional Alignment of Oxygen Molecules in Gaseous Expansions. *Nature* **1994**, *371*, 399–402, DOI: 10.1038/371399a0.

(46) Aquilanti, V.; Ascenzi, D.; Cappelletti, D.; Pirani, F. Rotational Alignment in Supersonic Seeded Beams of Molecular Oxygen. *J. Phys. Chem.* **1995**, *99*, 13620–13626, DOI: 10.1021/j100037a008.

(47) Lenzer, T.; Bürsing, R.; Dittmer, A.; Panja, S. S.; Wild, D. A.; Oum, K. Rotational and Vibrational Cooling in Pulsed High-Pressure Molecular Beam Expansions from 3 Bar into the Supercritical Regime. *J. Phys. Chem. A* **2010**, *114*, 6377–6383, DOI: 10.1021/jp9092207.

(48) Füchsel, G.; del Cueto, M.; Díaz, C.; Kroes, G.-J. Enigmatic HCl + Au(111) Reaction: A Puzzle for Theory and Experiment. *J. Phys. Chem. C* **2016**, *120*, 25760–25779, DOI: 10.1021/acs.jpcc.6b07453.

(49) Shirhatti, P. R.; Geweke, J.; Steinsiek, C.; Bartels, C.; Rahinov, I.; Auerbach, D. J.; Wodtke, A. M. Activated Dissociation of HCl on Au(111). *J. Phys. Chem. Lett.* **2016**, *7*, 1346–1350, DOI: 10.1021/acs.jpclett.6b00289.

(50) Liu, T.; Fu, B.; Zhang, D. H. Six-Dimensional Quantum Dynamics Study for the Dissociative Adsorption of HCl on Au(111) Surface. *J. Chem. Phys.* **2013**, *139*, 184705, DOI: 10.1063/1.4829508.

(51) Liu, Q.; Zhou, X.; Zhou, L.; Zhang, Y.; Luo, X.; Guo, H.; Jiang, B. Constructing High-Dimensional Neural Network Potential Energy Surfaces for Gas–Surface Scattering and Reactions. *J. Phys. Chem. C* **2018**, *122*, 1761–1769, DOI: 10.1021/acs.jpcc.7b12064.

(52) Füchsel, G.; Zhou, X.; Jiang, B.; Juaristi, J. I.; Alducin, M.; Guo, H.; Kroes, G.-J. Reactive and Nonreactive Scattering of HCl from Au(111): An Ab Initio Molecular Dynamics Study. *J. Phys. Chem. C* **2019**, *123*, 2287–2299, DOI: 10.1021/acs.jpcc.8b10686.

(53) Smeets, E. W.; Voss, J.; Kroes, G.-J. Specific Reaction Parameter Density Functional Based on the Meta-Generalized Gradient Approximation: Application to H_2 + Cu(111) and H_2 + Ag(111). *J. Phys. Chem. A* **2019**, *123*, 5395–5406, DOI: 10.1021/acs.jpca.9b02914.

(54) Rahinov, I.; Cooper, R.; Yuan, C.; Yang, X.; Auerbach, D. J.; Wodtke, A. M. Efficient Vibrational and Translational Excitations of a Solid Metal Surface: State-to-State Time-of-Flight Measurements of HCl(ν=2,J=1) Scattering from Au(111). *J. Chem. Phys.* **2008**, *129*, 214708, DOI: 10.1063/1.3028542.

(55) Geweke, J.; Shirhatti, P. R.; Rahinov, I.; Bartels, C.; Wodtke, A. M. Vibrational Energy Transfer near a Dissociative Adsorption Transition State: State-to-State Study of HCl Collisions at Au(111). *J. Chem. Phys.* **2016**, *145*, 054709, DOI: 10.1063/1.4959968.

(56) Díaz, C.; Olsen, R. A. A Note on the Vibrational Efficacy in Molecule-Surface Reactions. *J. Chem. Phys.* **2009**, *130*, 094706, DOI: 10.1063/1.3080613.

(57) Wijzenbroek, M.; Klein, D. M.; Smits, B.; Somers, M. F.; Kroes, G.-J. Performance of a Non-Local van Der Waals Density Functional on the Dissociation of H_2 on Metal Surfaces. *J. Phys. Chem. A* **2015**, *119*, 12146–12158, DOI: 10.1021/acs.jpca.5b06008.

(58) Smeets, E. W. F.; Kroes, G.-J. Designing New SRP Density Functionals Including Non-Local vdW-DF2 Correlation for H_2 + Cu(111) and Their Transferability to H_2 + Ag(111), Au(111) and Pt(111). *Phys. Chem. Chem. Phys.* **2021**, *23*, 7875–7901, DOI: 10.1039/D0CP05173J.

(59) Gross, A.; Wilke, S.; Scheffler, M. Six-Dimensional Quantum Dynamics of Adsorption and Desorption of H_2 at Pd(100): Steering and Steric Effects. *Phys. Rev. Lett.* **1995**, *75*, 2718–2721, DOI: 10.1103/PhysRevLett.75.2718.

(60) Roscioli, J. R.; Bell, D. J.; Nelson, D. J.; Nesbitt, D. J. State-Resolved Velocity Map Imaging of Surface-Scattered Molecular Flux. *Phys. Chem. Chem. Phys.* **2012**, *14*, 4070–4080, DOI: 10.1039/C1CP22938A.

(61) Luntz, A. C. A Simple Model for Associative Desorption and Dissociative Chemisorption. *J. Chem. Phys.* **2000**, *113*, 6901–6905, DOI: 10.1063/1.1311280.

(62) Yoder, B. L.; Bisson, R.; Beck, R. D. Steric Effects in the Chemisorption of Vibrationally Excited Methane on Ni(100). *Science* **2010**, *329*, 553–556, DOI: 10.1126/science.1191751.

(63) Yoder, B. L.; Bisson, R.; Morten Hundt, P.; Beck, R. D. Alignment Dependent Chemisorption of Vibrationally Excited $CH_4(\nu_3)$ on Ni(100), Ni(110), and Ni(111). *J. Chem. Phys.* **2011**, *135*, 224703, DOI: 10.1063/1.3665136.

(64) Morten Hundt, P.; Bisson, R.; Beck, R. D. The Sticking Probability of D_2O-Water on Ice: Isotope Effects and the Influence of Vibrational Excitation. *J. Chem. Phys.* **2012**, *137*, 074701, DOI: 10.1063/1.4742914.

(65) Pan, H.; Mondal, S.; Yang, C.-H.; Liu, K. Imaging Characterization of the Rapid Adiabatic Passage in a Source-Rotatable, Crossed-Beam Scattering Experiment. *J. Chem. Phys.* **2017**, *147*, 013928, DOI: 10.1063/1.4982615.

(66) Klaus, T.; Belov, S. P.; Winnewisser, G. Precise Measurement of the Pure Rotational Submillimeter-Wave Spectrum of HCl and DCl in Their $\nu = 0, 1$ States. *J. Mol. Spectrosc.* **1998**, *187*, 109–117, DOI: 10.1006/jmsp.1997.7465.

(67) Cazzoli, G.; Puzzarini, C. Hyperfine Structure of the J=1←0 Transition of $H^{35}Cl$ and $H^{37}Cl$: Improved Ground State Parameters. *J. Mol. Spectrosc.* **2004**, *226*, 161–168, DOI: 10.1016/j.jms.2004.03.020.

(68) Iwakuni, K.; Sera, H.; Abe, M.; Sasada, H. Hyperfine-Resolved Transition Frequency List of Fundamental Vibration Bands of $H^{35}Cl$ and $H^{37}Cl$. *J. Mol. Spectrosc.* **2014**, *306*, 19–25, DOI: 10.1016/j.jms.2014.09.013.

(69) Geweke, J. D. Scattering HCl Molecules from Au(111) and Ag(111) Surfaces, Lausanne: EPFL, 2019, DOI: 10.5075/epfl-thesis-9742.